NUREG/CR-3945
MEA-2055

Fatigue Crack Growth Rates of Low-Carbon and Stainless Piping Steels in PWR Environment

Prepared by W. H. Cullen

Materials Engineering Associates, Inc.

Prepared for
U.S. Nuclear Regulatory
Commission

GPO Printed copy price: $4.50

NUREG/CR-3945
MEA-2055
RF, R5

Fatigue Crack Growth Rates of Low-Carbon and Stainless Piping Steels in PWR Environment

Manuscript Completed: November 1984
Date Published: February 1985

Prepared by
W. H. Cullen

Materials Engineering Associates, Inc.
9700-B George Palmer Highway
Lanham, MD 20706

Prepared for
Division of Engineering Technology
Office of Nuclear Regulatory Research
U.S. Nuclear Regulatory Commission
Washington, D.C. 20555
NRC FIN B8900

ABSTRACT

Fatigue crack growth rates of A 106 Gr. C and A 516 Gr. 70 carbon steels, and A 351-CF8A stainless steel in PWR environments have been determined over a load ratio range (R) of 0.2 to 0.85, a temperature range of 93°C to 338°C, and a test frequency range of 17 mHz to 1 Hz using sinusoidal waveforms. In addition, growth rates have been determined for various orientations of the crack plane with respect to the product form. Crack growth rates in 288°C air environments have been measured in order to provide a reference baseline. These results define the magnitude of and major influences on the environmentally-assisted fatigue crack growth rates for these piping steels, and are supported by fractographic observations of the fatigue fracture surface.

Crack growth rates in A 106 Gr. C show the expected increase in growth rates with an increase in load ratio. At low load ratios, however, the growth rates also increase with a decrease in test frequency. At higher load ratios, there is little measureable frequency dependence. Over the temperature range of 93°C to 338°C, crack growth rates at R = 0.2 decrease by a factor of about six to eight. There is little, if any orientation difference between radial, circumferential and longitudinal crack growth directions.

Crack growth rates in A 516 Gr. 70, on the other hand, show a large and highly variable dependence on orientation. Fractographic studies indicate that this may be attributed to the density and distribution of the manganese sulfide inclusions in the steel. Most manganese sulfide inclusion sites on the fatigue fracture surfaces are surrounded by areas of brittle-like features which commonly characterize hydrogen-assisted subcritical crack growth in steel alloys. For this steel, growth rates at 1 Hz test frequency equaled those at 17 mHz for R = 0.2, and exceeded those at 17 mHz for R = 0.7, which is an inversion of "normal" behavior for steels in aqueous environments.

Crack growth rates in A 351-CF8A show more customary dependencies on load ratio and test frequency, specifically, growth rates increase with an increase in load ratio or a decrease in test frequency. Growth rates increase at both low and high temperatures and show very little environmental assistance in the range 200°C to 288°C. However, the fractographic examination showed brittle-like features on the fracture surfaces for those specimens which exhibited a large degree of environmental sensitivity, as well as those which did not.

CONTENTS

ACKNOWLEDGEMENT

The author would like to acknowledge the technical assistance of R. E. Taylor and C. L. Miller during the course of the autoclave testing aspects of this research. The air environment tests were conducted by E. d'Ambrosio. The SEM fractography was carried out at the Technical Research Centre of Finland (VTT) by M. Kemppainen, under the supervision of H. Hanninen and K. Torronen. Both the fractography and the suggestions of the VTT group have been of valuable assistance in these studies. M. E. Mayfield, of MEA, proofread the manuscript and contributed many helpful suggestions. The author appreciates the program leadership of F. J. Loss, of MEA, and the continued sponsorship of the U. S. Nuclear Regulatory Commission for their support of this research. The program manager for the NRC, M. Vagins, is to be thanked for his continued interest in all aspects of this research.

LIST OF FIGURES

LIST OF FIGURES

LIST OF FIGURES

1.0 INTRODUCTION, OBJECTIVE AND SCOPE

Research on the fatigue crack growth characteristics of pressure vessel and piping steels in pressurized, high-temperature, simulated reactor coolants is an important aspect of reactor safety assurance studies. Over the course of the 1970's, most of this work was focused on studies of pressure vessel steels -- A 533, A 508, and compatible welds and heat-affected zone specimens. As a result of that research, many important effects of critical variables have been identified. Among these are the effects of waveform and frequency, temperature steel composition, orientation, and water chemistry, especially dissolved oxygen content (Refs. 1-4). Many of these effects are not in accord with well-known trends, due to these same variables acting on structural steels in a marine environment, or pipeline steels in subterranean water (Refs. 5-9). Several recent reviews have focused on the fatigue crack growth of nuclear reactor pressure vessel steels in their applicative environments, and research is continuing on many yet unexplained phenomena (Refs. 10-11).

However, as the collection of data on pressure vessel steels increases, and the upper bounds of these data sets become better defined, some research interest has shifted to the piping steel question. The objective of this study was to measure fatigue crack growth rates (FCGR) on low-carbon and stainless steels in a simulated pressurized water reactor environment. The results described below are from an ongoing scoping study, and describe effects of load ratio, temperature and orientation on FCGR results. The scope of this effort was confined to testing on SA 351-CF8A cast stainless steel, A 106 Gr. C and A 516 Gr. 70 carbon steels. In each case, only particular variables were selected for the test matrix. This series of tests was not intended to be an exhaustive matrix to cover both materials and critical variables. The steels selected are in wide use, and this compilation of data provides an index of the fatigue crack growth behavior of these steels relative to the more-investigated pressure vessel steels.

Some fatigue crack growth rate data on stainless piping steels in PWR environments have been published previously. Bamford has published results of a frequency and load rate study which shows the usual increases in growth rates vs. applied cyclic stress intensity factor with increasing load ratio and decreasing test frequency (Ref. 12). Amzallag has published the initial results of a study of aging effects in cast stainless steels, and has shown that aging (7500 hours at 400°C) does lead to a significant increase in growth rates (Refs. 13-15). Hale and associates at General Electric-San Jose have been working with low-carbon and stainless piping steels for several years and have released several series of reports documenting effects found at very low cyclic periods (Ref. 16). Coffin and Prater at General Electric-Schenectady have described results in part-through crack geometries, showing the effects of environment on crack shape and growth rates (Refs. 17-19). Nearly all of the General Electric research has been with water containing various amounts of dissolved oxygen, simulating the various phases of BWR operation.

2.0 SPECIMENS, FACILITIES DESCRIPTION AND TEST PRACTICE

2.1 Specimens and Materials

The parent material for this study came in three different forms. The A 106 Gr. C came as rings which were 0.81-m (O.D) x 0.2-m long and 83-mm thick (32 in. x 8 in. x 3-1/4 in.). There were two shipments of A 106 received and used in this program. Specimens with serial codes FOP-57 through FOP-62 were from Lot #1; specimens FOP-63 through FOP-94 were from Lot #2. The A 516 Gr. 70 came as a plate which was 0.4 m x 0.9 m x 0.15 m (16 in. x 36 in. 6 in.). The A 351-CF8A was a segment from a research pressure vessel which was 0.8 m (32 in.) in diameter and 57-mm (2-1/4-in.) thick.

Compact specimens and the two-pin, wedge-opening load (CT and WOL) specimens were used throughout this research. Specimens were 25.4-mm or 50.8-mm (1-in. or 2-in.) thick (1T- or 2T-) with machined notches to a normalized depth (crack length to width, or a/W) of 0.25 to 0.35. In all cases, the specimens were precracked in air by at least 1.2 mm (for 1T specimens) or 2.5 mm (for 2T specimens) at a low ΔK with respect to the initial ΔK of the actual test. The size of the specimens, orientation with respect to the rolling direction and other pertinent information is contained in captions of the appropriate figures. Figure 1 shows a schematic of the orientation codes, in relation to the product form, which are taken from ASTM E 399. The material chemistries are given below in Table 1.

Table 1 Chemical Composition of the Low-Carbon Piping Steels Examined in this Study

Element	C	S	Si	Mo	Ni	Mn	Cr	V	P
A 106 Gr. C Code FOP									
Lot #1	0.25	0.017	0.22	0.033	0.25	0.88	0.10	0.003	0.016
Lot #2	0.25	0.016	0.18	0.049	0.26	0.92	0.22	0.003	0.018
A 516 Gr. 70 Code FOK	0.25	0.017	0.23	0.065	0.27	1.05	0.10	0.002	0.018
A 351-CF8A Code A9	0.06	0.018	1.17	-----	8.58	0.68	20.42	-----	0.020

2.2 Test Facilities

All tests were conducted under load-controlled, constant amplitude cycling. Specimens were tested in ovens, for air tests, or in environmental chambers which contain the simulated reactor coolant environments under the required temperature and pressure conditions.

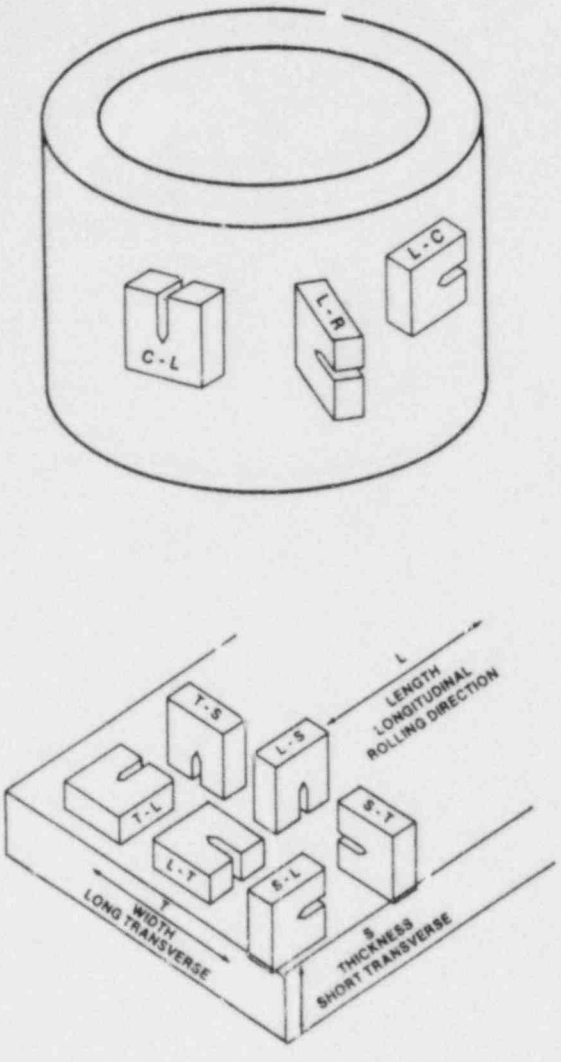

Fig. 1 A schematic showing the orientation nomenclature used in this report. This is the standard nomenclature from ASTM E 399.

Both single specimen tests and multiple-specimen, daisy chain tests were utilized in these studies. The multiple-specimen test technique has been described previously (Ref. 20).

Air tests were conducted in resistance-heated convection ovens with a control thermocouple mounted in the wall of the oven and monitoring thermocouples spot-welded to the specimen itself. An LVDT* was attached to the specimen front face in order to determine crack mouth opening. In the case of the water environment tests at 93°C, a 6-liter capacity, stainless steel vessel, equipped with an internal LVDT, and a dedicated water circulation loop was employed. This chamber was kept at the slightly positive pressure of 35 kPa, using nitrogen as a cover gas in the feedwater tank. This chamber was mounted in a 55-kN (10-kip) four-column load frame. Only 1T specimens were tested in this system.

In the case of tests at higher temperatures, autoclaves capable of containing pressurized water were used. Two such autoclave systems were utilized in this study. The smaller of the two contained four liters of water; the larger was a three-chamber, multispecimen system with each autoclave accomodating four specimens and holding about 150 liters of water. The small autoclave is capable of 55-kN loads and the larger autoclaves are capable of 550-kN (10-kips and 100-kips. respectively); an LVDT was attached to each specimen. Both systems operated in essentially the same way. Water from a feedwater tank is pressurized to 13 to 18 MPa, preheated and pumped to the autoclave. Water returning from the autoclave is cooled in a heat exchanger, passed through a pressure-control valve and returned to the feedwater tank. Each feedwater tank is equipped with a separate loop for on-line evaluation of dissolved oxygen content, pH and conductivity of the water. More complete details and illustrations of these systems can be found in Reference 21.

The water for these autoclave tests is prepared by piping city water through four mixed-bed ion exchange columns and into a storage tank. Two hundred-liter quantities of this water are then pumped to a second container and mixed with the boric acid and lithium hydroxide to produce the nominal chemistry shown in Table 2. During the test, these systems are monitored on-line for pH, conductivity and dissolved oxygen. Grab samples are taken at occasional intervals to check for chloride and fluoride content. More recent, and far more accurate analyses indicate that chloride contents may have been in the range of 150 to 200 ppb, or a factor of about 2 over the specification. In addition, sulfate contents (for which there is no specification) were probably between 100 and 150 ppb. Recent results from the UKAEA laboratories at Harwell, which are not yet available as a reference, suggest that relatively low levels of sulfate do not affect growth rates, but that 1000-ppb levels, attained by deliberate additions of sulfuric acid to the autoclave environment, may have a significant effect on the growth rates. A recent result from Van Der Sluys (Ref. 22) indicates that deliberate addition of 135 ppb chloride ion

---

* Linear Variable Differential Transformer

did not increase crack growth rates at a test frequency of 10 mHz in a specimen containing 0.025% S.

Table 2 Water Chemistry Specifications

Boron (as boric acid)	1000 ppm
Lithium (as lithium hydroxide)	1 ppm
Chloride ions	< 0.15 ppm
Fluoride ions	< 0.10 ppm
Dissolved oxygen	~ 1 ppb
Dissolved hydrogen (saturation)	30 to 50 cm^3/kg water

All other metallic or ionic species should be at about trace levels. Some iron, both in solid and soluble form is the inevitable result of a corroding specimen.

A computerized data acquisition system was used to measure the crack mouth opening displacements, loads, cycle counts and water chemistry parameters during the course of the tests. Crack lengths were computed from standard specimen compliance to crack length equations (Ref. 23). A complete description and illustrations of these systems can be found in References 21 and 24.

2.3 Test Practice and Data Processing

Each specimen was mounted in the oven or autoclave system and exercised at low load to assure that the servohydraulics, displacement gage, and data acquisition systems were in good working order. Following this, the autoclave chamber was bolted shut and filled with water. The low temperature system was filled with deoxygenated water directly from the feedwater tank. For the high-temperature water systems, the temperature was brought to 93°C (200°F) for about 12 hours in order to partially deoxygenate the water. The high temperature systems were then pressurized and the water was allowed to circulate back to the feedwater tank until fully deoxygenated. The temperature was then brought to the desired value.

Tests in 288°C air environment were conducted at 1 Hz. Some aqueous environment tests were also conducted at 1 Hz as indicated below. Other aqueous environment tests were begun by cycling at 1 Hz at the desired test loads to achieve about 5 mm of crack extension. The purpose of this practice is threefold. First, the crack is extended into a region of higher stress intensity factor (K) gradient, which means that a proportionally larger range of ΔK can be covered with less crack extension and hence, less test time. Secondly, useable data sets are produced, and many of them are plotted and described in the next section. Lastly, the cycling at 1 Hz might provide some environmental conditioning of the specimen or the water in the crack-tip enclave. This latter consideration has no proven basis at the present time, but it appears to be a beneficial procedure.

In the case of the tests in the multispecimen autoclaves, the test is periodically interrupted as each specimen reaches the desired terminal crack length. At each interruption, the loads are reduced to about 50% of the test values, the frequency is increased to 1 Hz, and the cycling is applied until the specimen being terminated has completely broken. Under the usual circumstances, the specimens remaining in the daisy chain exhibit little or no crack growth. Although crack growth is monitored during this phase, it is not considered valid because of the significant reduction in loads. These data sets are not included in the following plots unless that is specifically indicated.

During the course of the test, the data acquisition system acquires four or five times the amount of data which will actually be used in the final calculation of the crack growth data set. This is principally to assure that no significant aspect of the test will be missed. After completion of the test, each data set is purged of excess data in order to meet the criteria for increments between crack lengths as presented in ASTM Standard E 647 (Ref. 25). Each specimen is measured for initial and final crack length and any significant beachmarks in between, and the data sets are post-test corrected using the methodology described in Reference 20.

Throughout this report, fatigue crack growth data are most often plotted in two ways:

(1) Log (da/dN) vs. ΔK -- fatigue crack growth rate vs. applied cyclic stress intensity factor. This is the most conventional method of plotting crack growth rates which have been developed using fracture mechanics type specimens such as CT or WOL specimens. This type of plot has the advantage that it shows the stress-based variable which is needed in most engineering calculations. But it does not show time-based phenomena which may be compounded with the crack growth rates, nor does it show any time-based comparison of two or more specimens in a multiple specimen test. As with all environmentally-assisted mechanical testing, graphs such as these are subject to the misinterpretation that ΔK is the only independent variable. Indeed, this is borne out by some of the data sets shown later in this report, for which two nominally identical tests exhibit a factor of twenty difference in crack growth rates, at the same value of ΔK. This difference may be due to microstructural influences, many of which are not well understood at the present time.

(2) Log (da/dN) vs. N -- crack growth rate vs. cyclic count. This graph is very useful for the intercomparison of specimens in a multispecimen test, or for the determination of the time-wise response of the specimen to changes in the test parameters. This type of graph will be used to show that stainless steel specimens can exhibit a large degree of environmental assistance at the same time that low-carbon steel specimens are exhibiting little environment effect. This graph does not convey any information about crack growth rate dependence on ΔK. It is also very easy to indicate the occurrence of significant incidents during the conduct of the test, such as changes in

load or test frequency values, or interruptions which may induce transients in the growth rate data.

3.0 RESULTS AND DISCUSSION

3.1 Low-Carbon Steels -- A 106 Gr. C and A 516 Gr. 70

3.1.1 Frequency and Load Ratio Effects

Data sets which describe effects of frequency, load ratio, orientation, and temperature are included below. In order to establish a baseline against which to compare the aqueous environment test results, 288°C air tests, using a load ratio (R) of 0.2, were conducted on specimens of each of these steels. Those results are shown in Figs. 2a and 2b. In subsequent figures, these essentially linear results are represented by a line which referenced the best fit through the air environment data. Crack growth data trend lines from other published research (Refs. 26-28) on A 516 and A 106 Gr. B are included in Fig. 2. Figure 3 shows results from 1-Hz tests on five specimens of A 106 in a water environment. The data sets, for load ratios of 0.125, 0.2 and 0.7, show the usual load ratio effect, in which higher load ratios show higher growth rates at lower ΔK values. However, there is a strong indication that for all load ratios, the data sets bend over to the right, as ΔK increases, and that the growth rates for all load ratios may blend together at some higher value of growth rate which was out of the range of this investigation. Figure 4 shows data for a 17-mHz sinusoidal waveform and load ratios of 0.2 and 0.7. Here the separation due to load ratio is clearly evident, but in the case of the data for FOP-61, there is a noticable bending over of the data set at the highest growth rates, indicating that the rapid increase in growth rates with ΔK cannot be sustained.

Figures 5 through 8 show a feature which recurred rather often, especially at the higher load ratio. In many cases, the crack growth rates at the high test frequency were higher than the growth rates for the lower frequency. Normally, the somewhat timewise-dependent environmental aspects of these tests causes the opposite result. Figure 5 shows a da/dN vs. ΔK plot for specimen FOP-60, in which the overall higher growth rates at the 1-Hz test frequency can be seen. A similar test on specimen FOP-61 produced somewhat more ambiguous results, shown in Fig. 6. Figures 7 and 8 are plots of crack growth rates vs. cyclic count in which the differences can be seen more clearly. Unlike the test of FOP-60, the test of FOP-61 was conducted in two stages, separated by a long residence of the specimen outside the autoclave. Although the initial phase of testing of specimen FOP-61 at 1 Hz showed a tendency toward high growth rates, the subsequent test phases seem to blend together, showing little effect of frequency. Comparison of 1-Hz and 17-mHz data for specimen FOP-62 in Fig. 4, tested at load ratio of 0.2, shows that these data sets also blend together with little dependence on frequency. Many other data sets for R = 0.2, presented later in this report, exhibit the same feature.

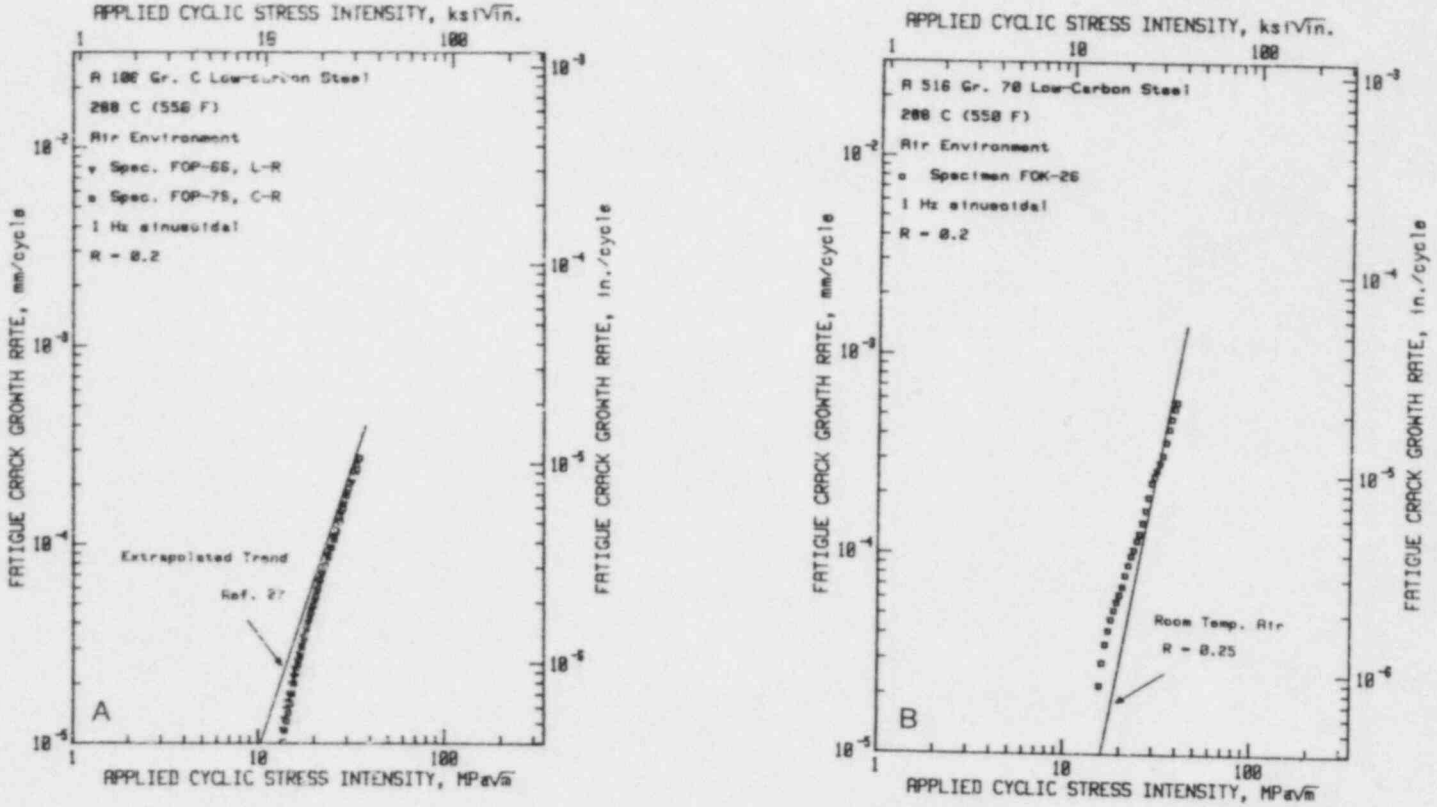

Fig. 2 Fatigue crack growth rates vs. applied cyclic ΔK for A 106 Gr. C and A 516 Gr. 70 steels for 288°C (550°F) air environment, and a test frequency of 1 Hz at a load ratio of 0.2. In companion figures later in this report, these data sets are illustrated by the best linear fit. Also shown are trend lines from other reports of studies on similar steels (Refs. 26-28).

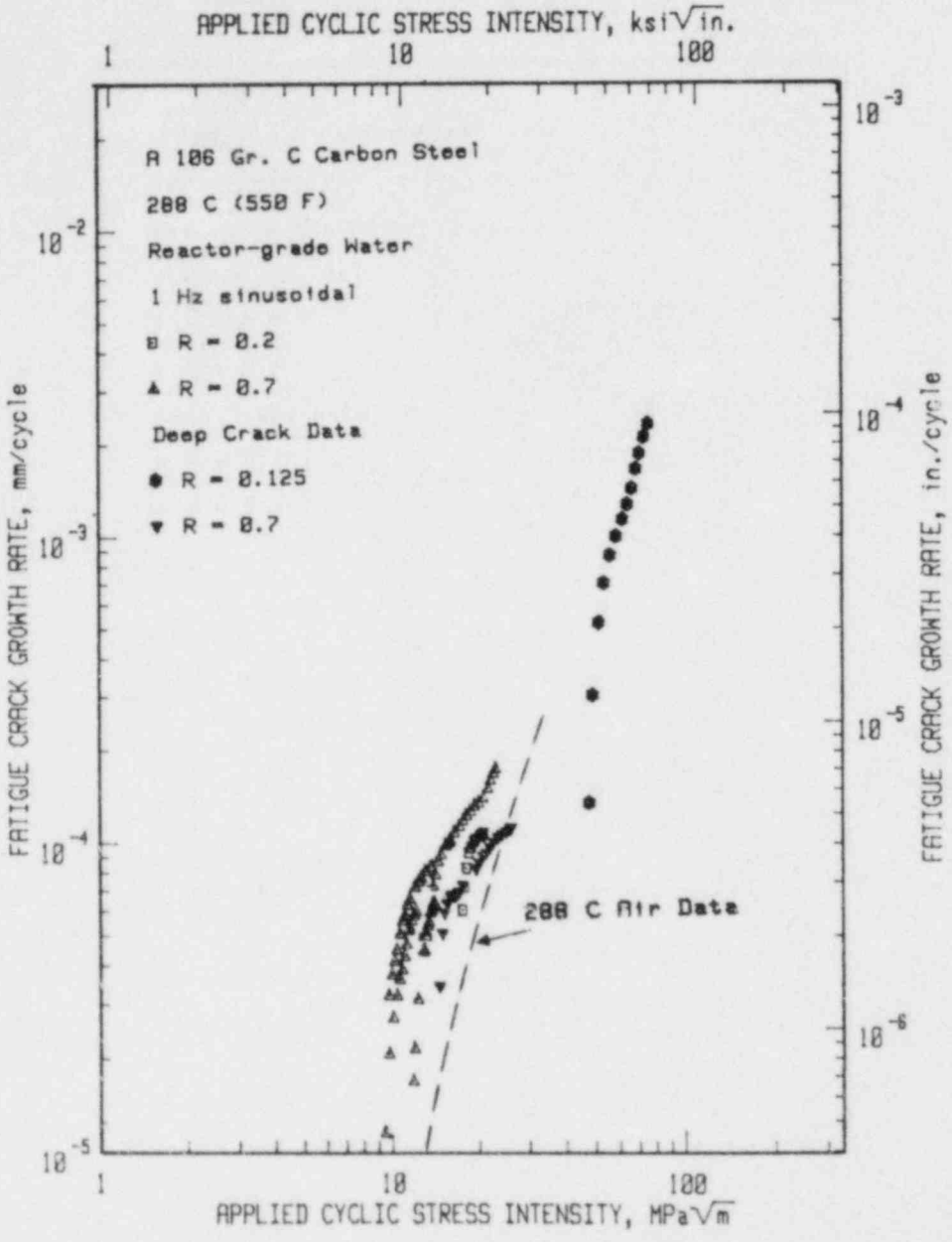

Fig. 3 Fatigue crack growth rates vs. applied cyclic ΔK for A 106 Gr. C steel in 288°C PWR environment, for a test frequency of 1 Hz, and load ratios of 0.125, 0.2 and 0.7. Note that the two specimens tested with deep cracks exhibited uncharacteristically low crack growth rates.

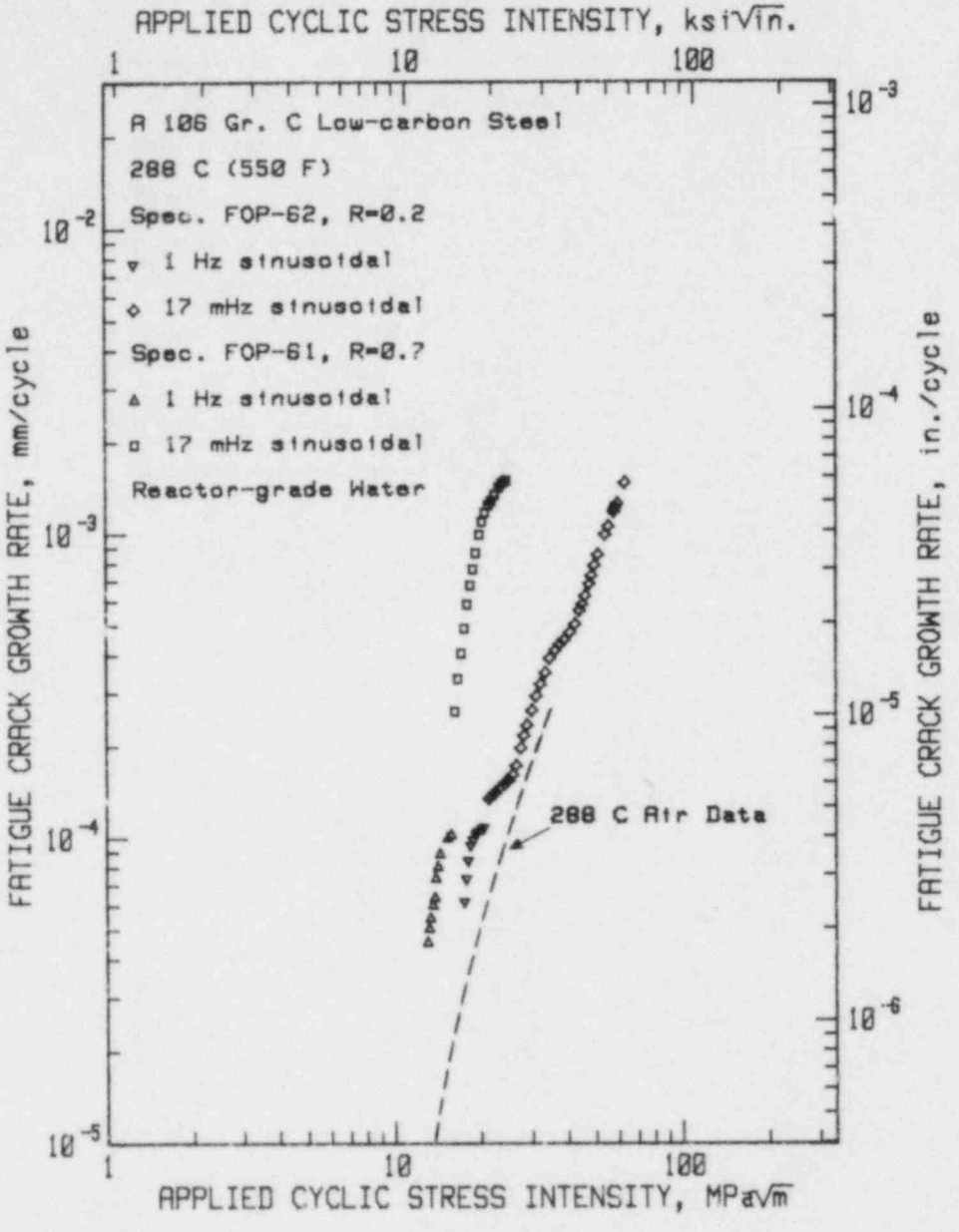

Fig. 4 Fatigue crack growth rates vs. applied cyclic ΔK for A 106 Gr. C steel in 288°C PWR environment, for load ratios of 0.2 and 0.7.

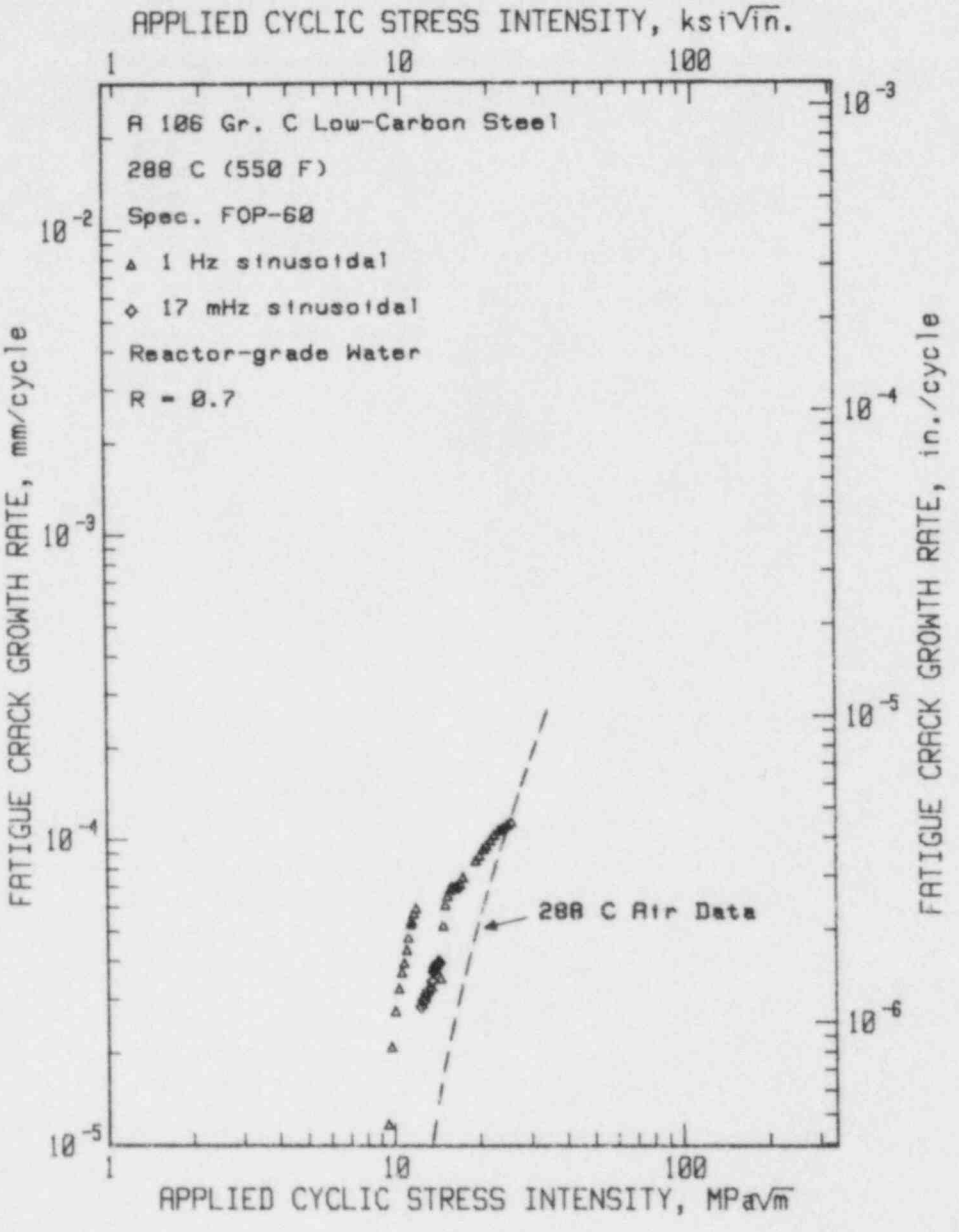

Fig. 5 Fatigue crack growth rates vs. applied cyclic ΔK for A 106 Gr. C steel for test frequencies of 1 Hz and 17 mHz, and a load ratio of 0.7. These data show that growth rates at 17 mHz are slower than growth rates at 1 Hz.

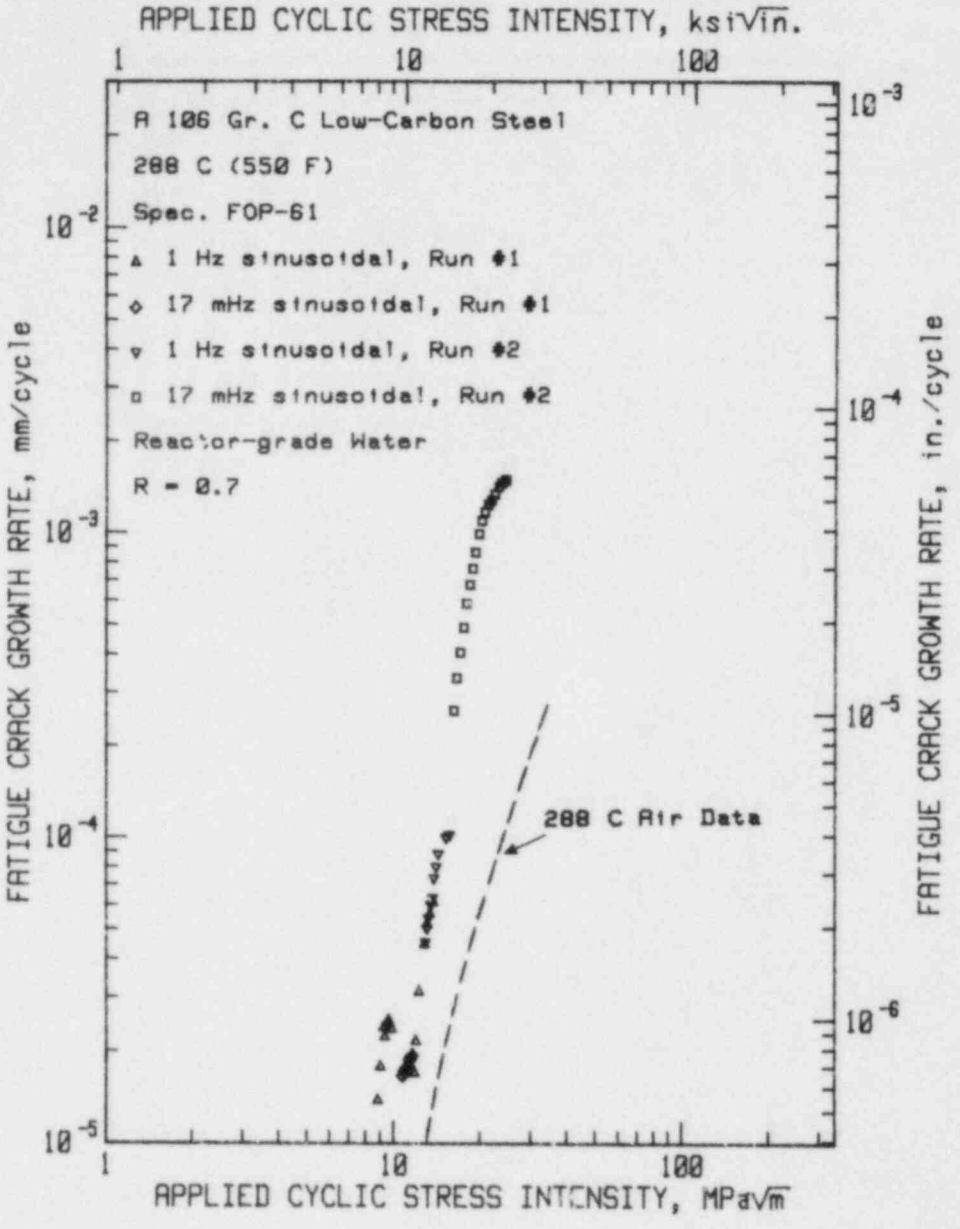

Fig. 6 Fatigue crack growth rates vs. applied cyclic ΔK for A 106 Gr. C steel in PWR environment for test frequencies of 1 Hz and 17 mHz, and a load ratio of 0.7. These data show that growth rates at 1 Hz were faster than growth rates at 17 mHz during run #1, but the reverse was true during run #2.

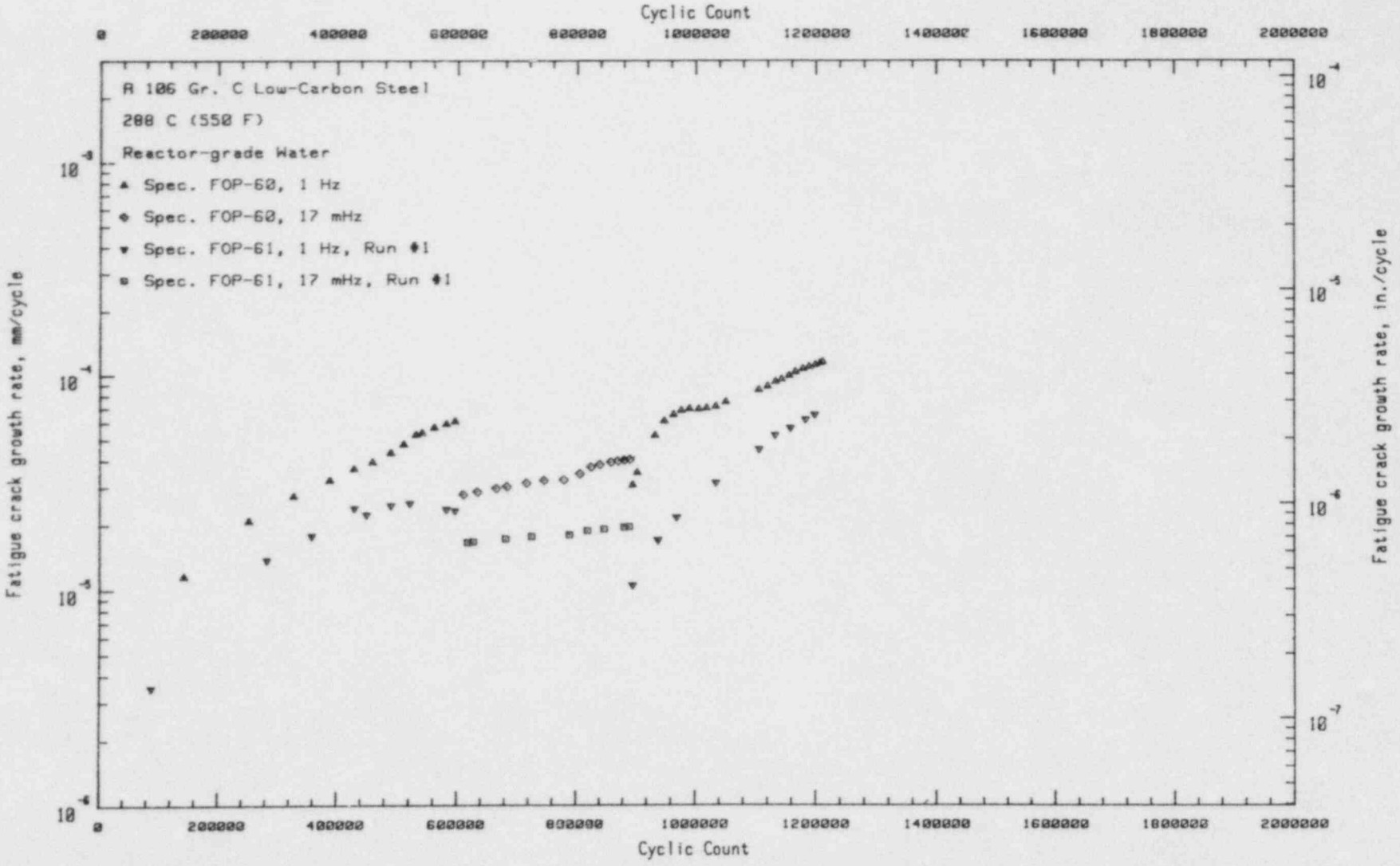

Fig. 7 Fatigue crack growth rates vs. crack length for multispecimen tests including two specimens of A 106 Gr. C steel for test frequencies of 1 Hz and 17 mHz, and a load ratio of 0.7. These are some of the same data sets as in Figs. 5 and 6.

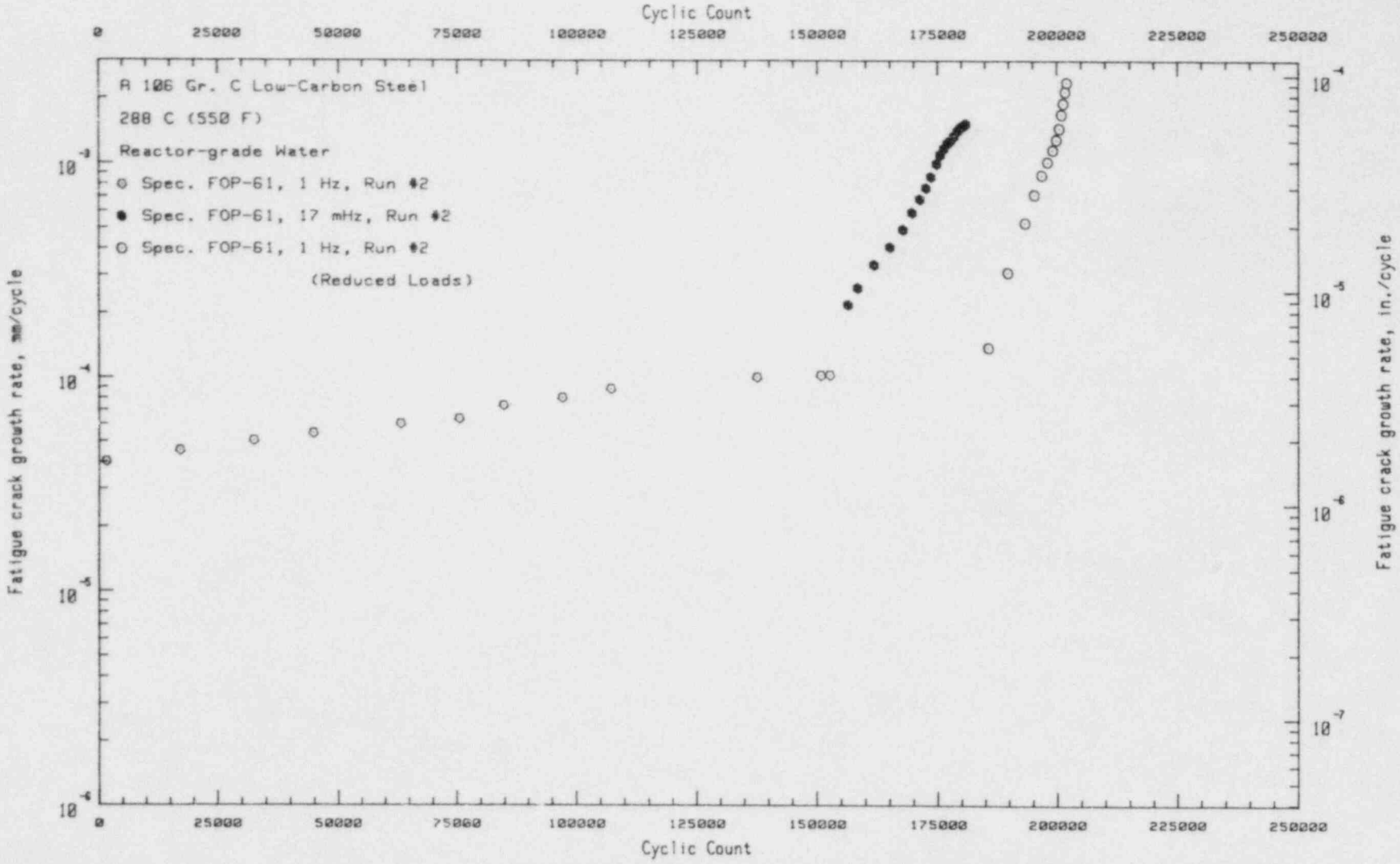

Fig. 8 Fatigue crack growth rates vs. crack length for a specimen of A 106 Gr. C, also shown in Fig. 6. In this case, the growth rates at 17 mHz were faster than those at 1 Hz.

Similar results for A 516 are shown in Figs. 9 and 10. Figure 9 shows data for a 1-Hz test frequency for two orientations of the crack plane, together with 288°C trend line for air results on the same steel. These results demonstrate that there can be a significant environmental effect even at the relatively high test frequency of 1 Hz. Figure 10 contains data from 2T specimens for both 1-Hz and 17-mHz test frequencies, and load ratios of 0.2, 0.7 and 0.85, the last for a test frequency of 50 mHz. There is a general layering of the data sets as a function of load ratio. The 1-Hz and 17-mHz data sets for the R = 0.2 test (specimen FOK-16) blend together quite smoothly, and although the 17-mHz portion started out at slightly lower growth rates than the 1-Hz portion, higher growth rates for the lower test frequency were quickly attained and a maximum in environmental assistance was reached in the midrange of applied ΔK, at about 28 MPa$\sqrt{m}$. Growth rate trends then bend over and slow appreciably. There is a greater degree of variability evident in the results for R = 0.7. The growth rates at 17 mHz for specimens FOK-11 and FOK-13 show a difference of a factor of about 10, which is likely due to a difference in material properties, such as microstructure, since the test practice and environments were essentially the same, although the tests were not conducted at exactly the same time. It is important to note that specimens FOK-11 and FOK-13 are of the same orientation, and in fact were cut from neighboring locations at the same elevation from the parent plate. These common denominators suggest that such variability and the consequent differences in growth rates are difficult characteristics to predict.

The results of the load ratio aspects of this part of the study are quite clear in that higher load ratios produced higher growth rates for equivalent ΔK values, with a trend toward bending over at the higher growth rates. The results of the frequency study are less clear in that for load ratios of 0.7 test frequencies of 1 Hz often produced higher growth rates than test frequencies of 17 mHz.

3.1.2 Temperature Effects in A 106 Gr. C

A study of the effects of temperature on growth rates in A 106 yielded the data sets shown in Figs. 11 through 13, and the trend line plot in Fig. 14. The 93°C data in Fig. 11 were acquired on 1T-CT specimens in a single-specimen test device, while data sets at the higher temperatures were collected from 2T-CT specimens. It is clear from these figures that the growth rates are lowest at the highest temperature, which is typical of primary circuit hot leg operating temperatures. The results from these two A 106 steel specimens tested at 338°C were generated simultaneously in a multiple-specimen test in which two stainless steel specimens (SA 351-CF8A) were also tested. Interestingly, while these two carbon steel specimens were cracking at rates which approximate air environment rates, the two stainless steel specimens were fatigue cracking at rates showing a rather high degree of environmental sensitivity. This is most clearly seen in Fig. 15, which is a plot of crack growth rates vs. cyclic count for the entire multiphase, multiple-specimen test. This figure shows that for those earlier phases of the test, during which the stainless steel specimens were producing high growth rates, the low-carbon steel specimens were

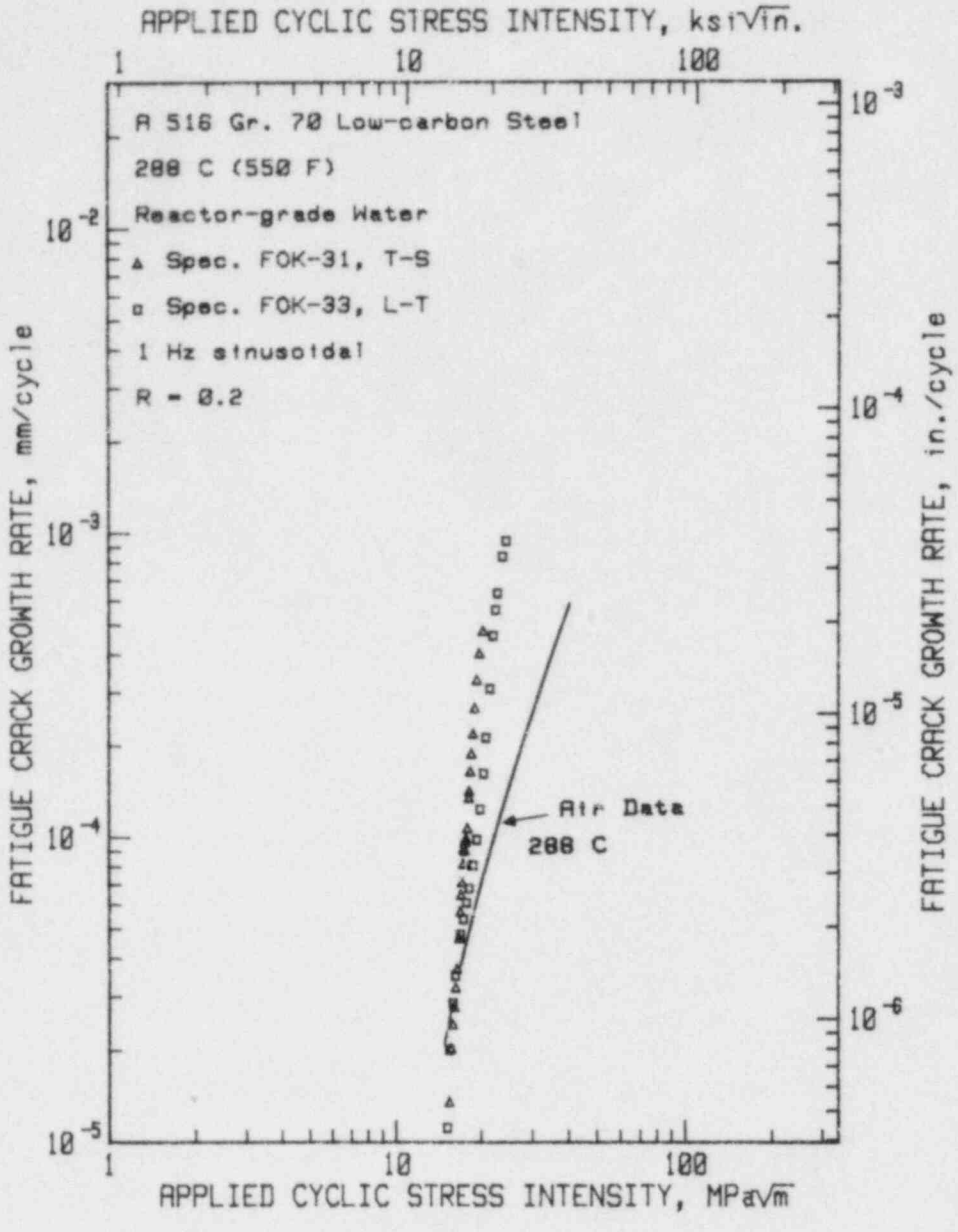

Fig. 9 Fatigue crack growth rates vs. applied cyclic ΔK for A 516 Gr. 70 steel in PWR environment for a test frequency of 1 Hz and a load ratio of 0.2. There is little apparent orientation dependence for these data sets, but comparison with the air data shows a considerable environmental component.

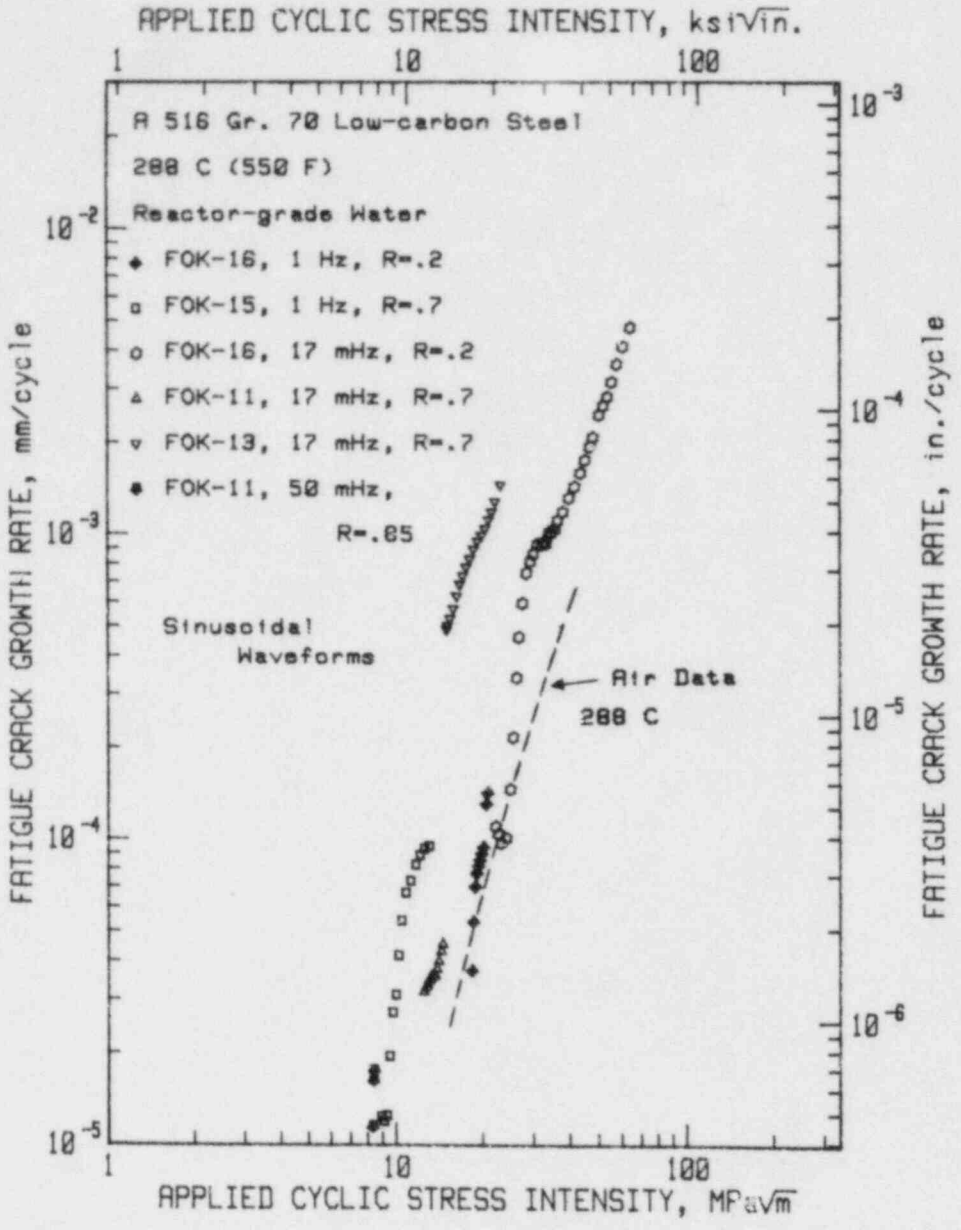

Fig. 10 Fatigue crack growth rates vs. applied cyclic ΔK for A 516 Gr. 70 steel in 288°C PWR environment for various test frequencies and load ratios.

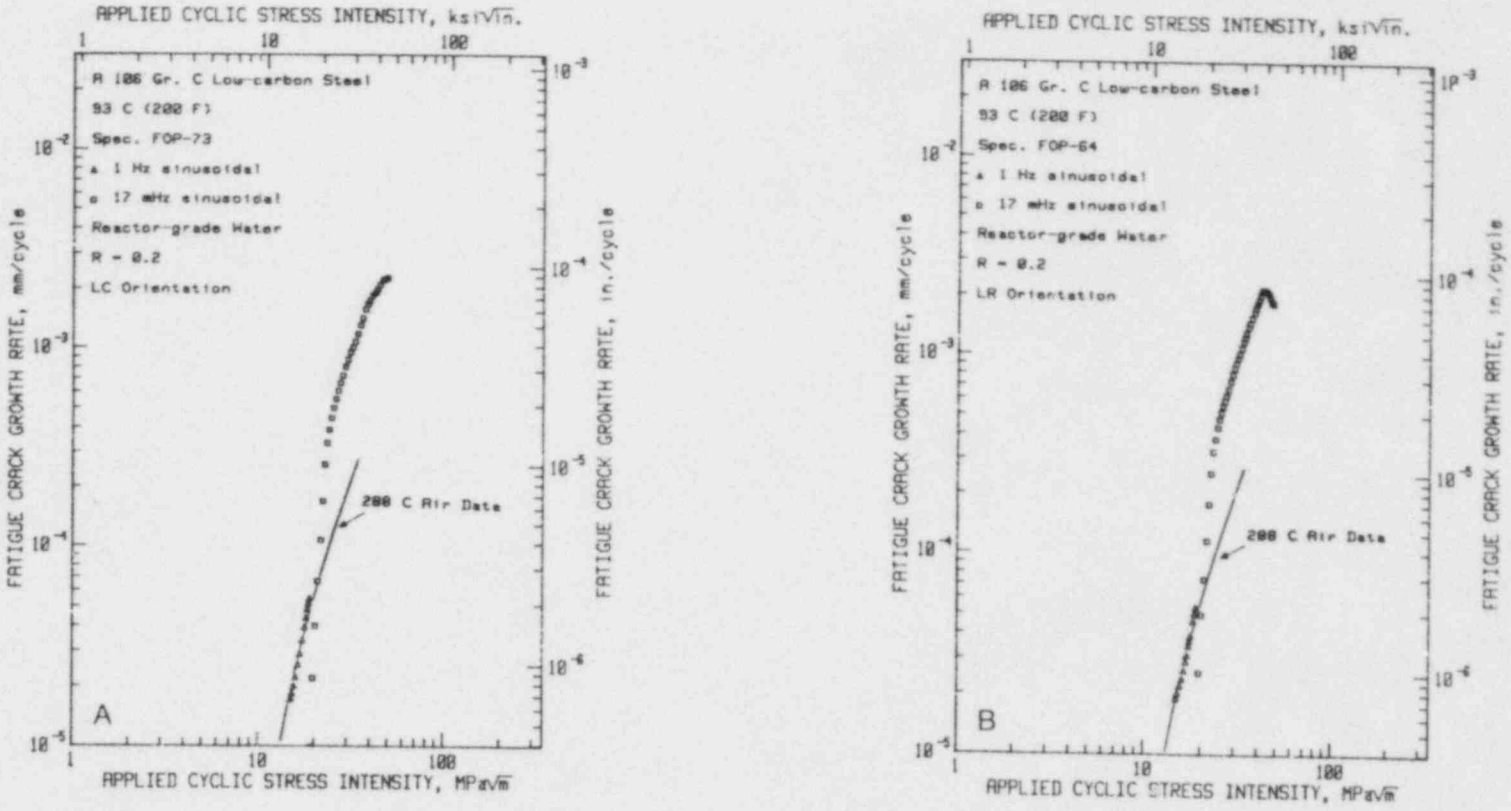

Fig. 11 Fatigue crack growth rates vs. applied cyclic ΔK for A 106 Gr. C steel in 93°C PWR environment at 1 Hz and 17 mHz frequencies and a load ratio of 0.2. There is no measurable orientation difference between the two specimens(L-C in a and L-R in b), but there is a considerable environmental enhancement at both test frequencies.

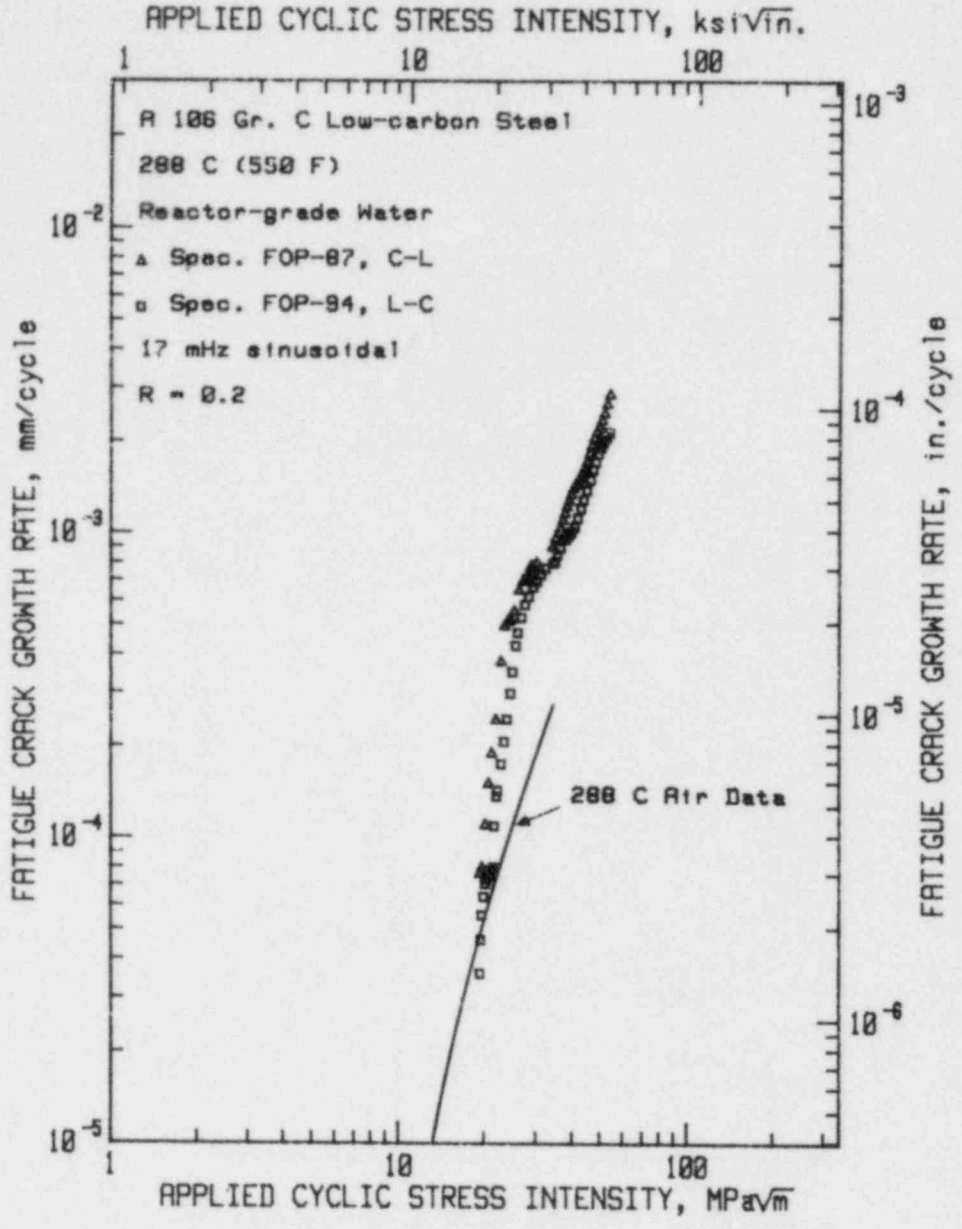

Fig. 12 Fatigue crack growth rates vs. applied cyclic ΔK for A 106 Gr. C steel in 288°C PWR environment for 17 mHz test frequency. There is no measurable orientation dependence between the two specimens.

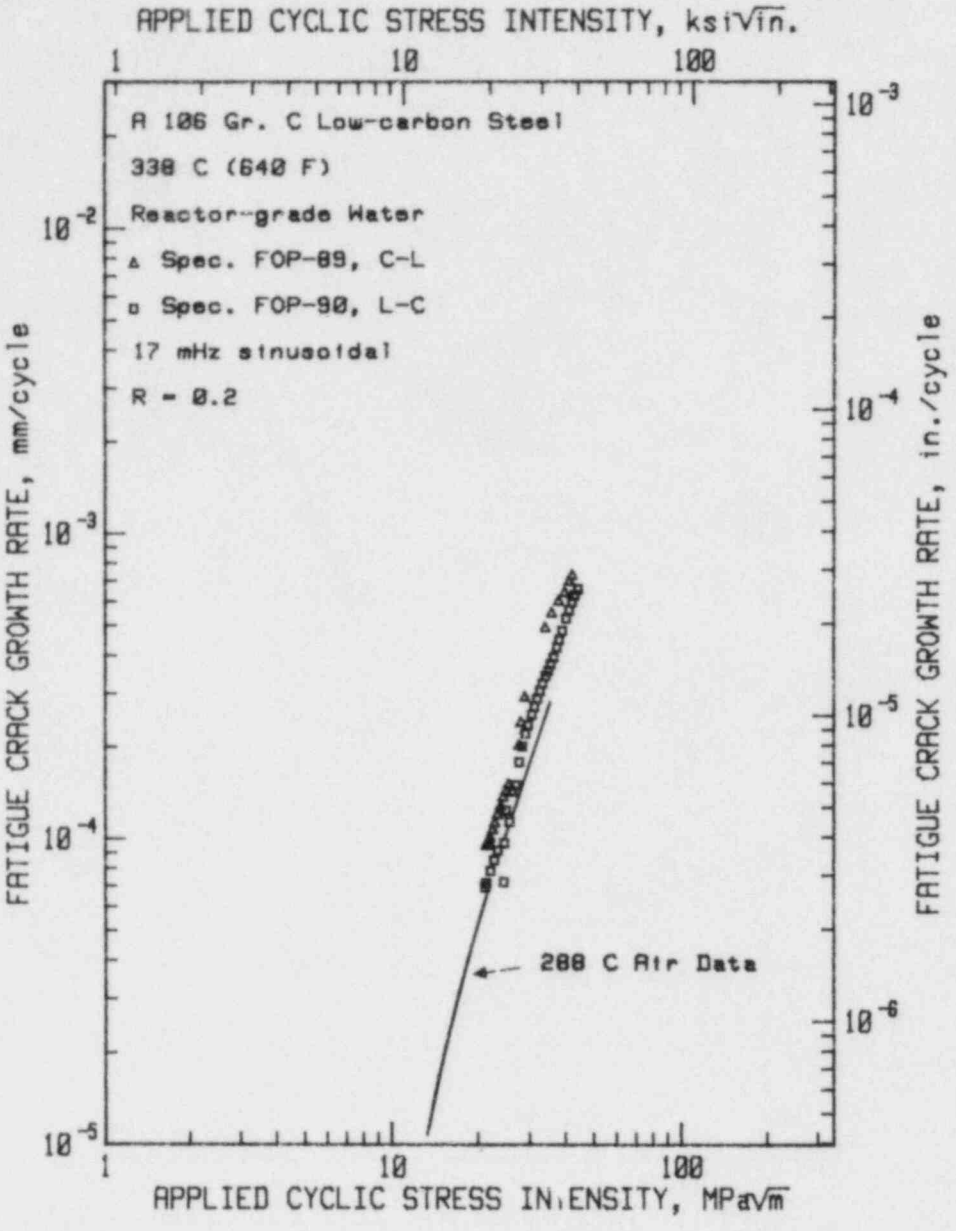

Fig. 13 Fatigue crack growth rates vs. applied cyclic ΔK for A 106 Gr. C steel in 338°C PWR environment, for a test frequency of 17 mHz, and a load ratio of 0.2. There is virtually no environmental enhancement shown in these growth rates.

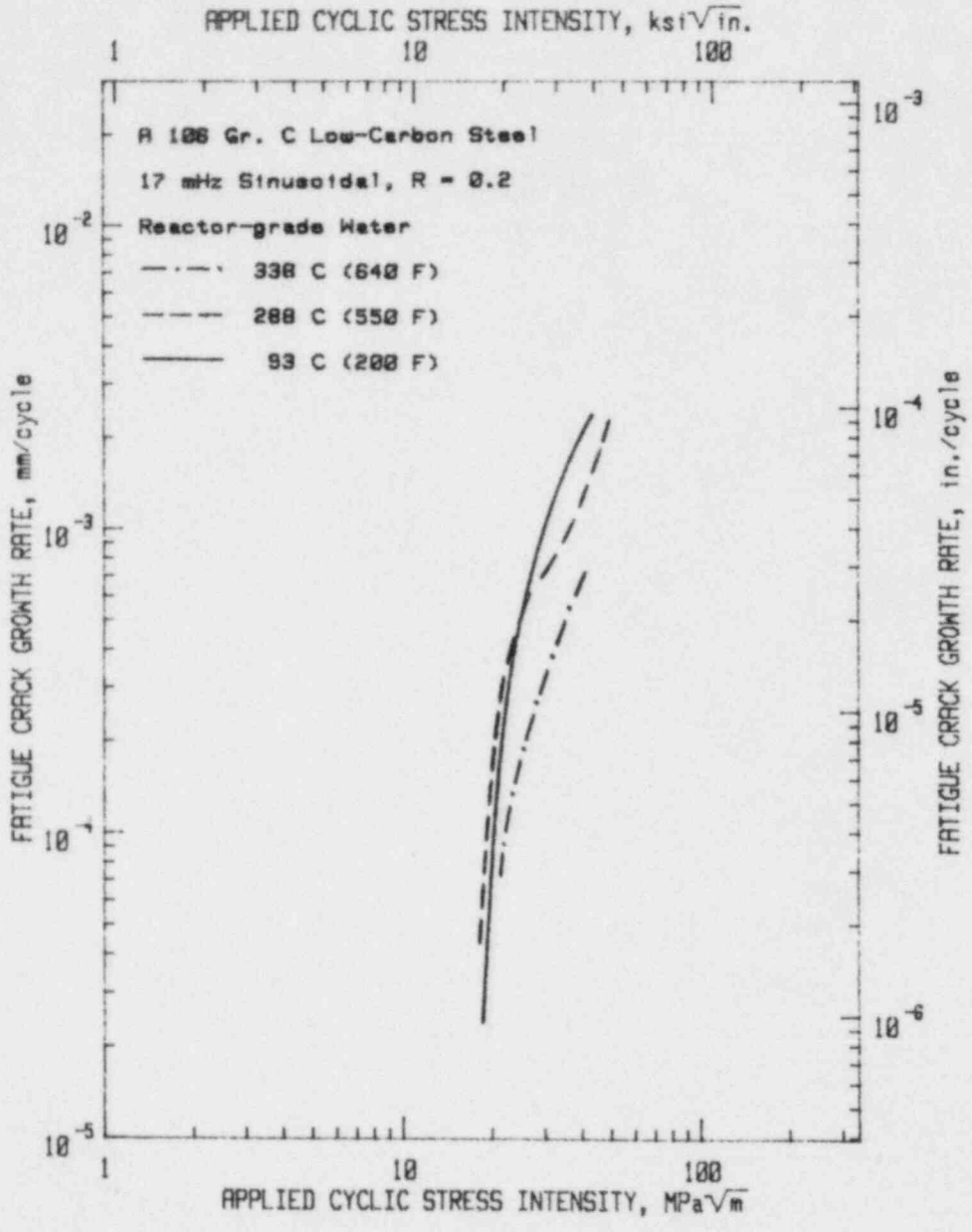

Fig. 14 Trend lines for the fatigue crack growth rate data sets shown in Figs. 11, 12 and 13. The test results for 338°C exhibit the lowest crack growth rates.

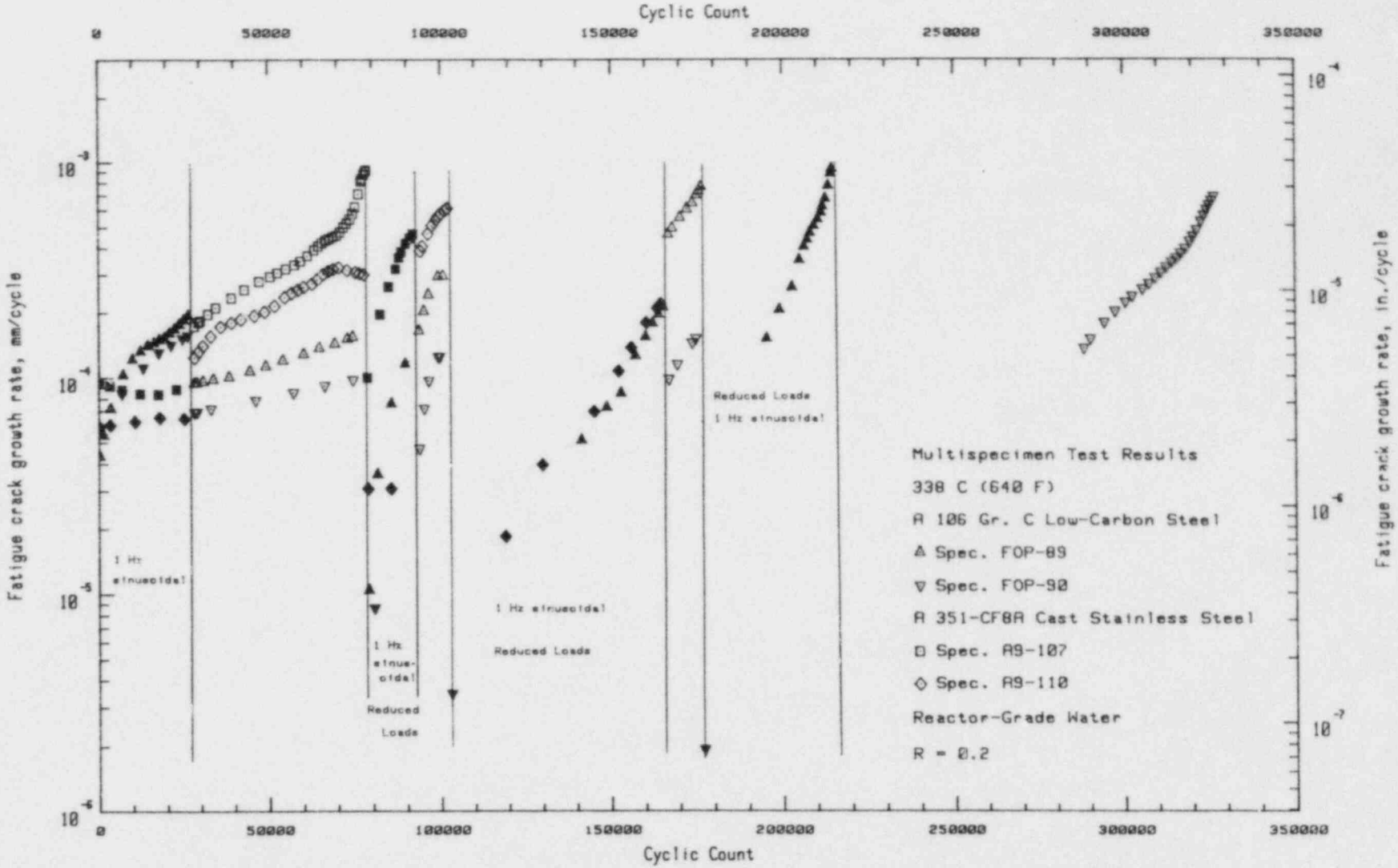

Fig. 15 Fatigue crack growth rates vs. cyclic count for the four specimens in a multi-specimen test, including the two specimens from Fig. 13 which showed low growth rates. Note that while the A 106 steel specimens were showing low growth rates, the A 351-CF8A cast stainless specimens (shown in Fig. 35 in this report) were exhibiting high growth rates. Darkened symbols are data sets for the 1 Hz portions of the test.

showing very little growth at all. This figure also shows that for the very first, 1-Hz phase of the test program, the carbon steel specimens showed rather high growth rates, while the stainless steel specimens showed low growth rates. Upon conversion to a 17-mHz test frequency, this trend completely reversed. These results imply that there were no significant problems with the test practice for this test, and that the low growth rates on the carbon steel, and the higher growth rates on the stainless steel are both correct and free from any interference from overloads or unknown environmental transients.

In an earlier report on temperature effects in A 508-2 pressure vessel steel (Ref. 29). the author showed that a minimum in growth rates was developed at a temperature of about 200°C (~ 390°F). By plotting these results in a similar way, as a function of inverse temperature, the degree of this effect can be seen in Fig. 16. The dotted line shows the previously published trend for A 508-2. The piping steel trend lines indicate that the magnitude of the trend is somewhat similar to that for the pressure vessel steel, but displaced to a higher temperature. The increase in growth rates, if any, would occur at unattainable combinations of pressure and temperature, and do not bear on any realistic operating transient scenarios. While data sets for two orientations of the crack plane are shown in each of the above figures, there is no discernible dependence of the crack growth rates on this orientation difference.

3.1.3 Orientation Effects in A 516 Gr. 70

1T-CT specimens were cut from a plate of A 516 Gr. 70 with various orientations of the crack plan relative to the rolling direction of the plate. These specimens were all tested at 288°C, using a combination of 1-Hz and 17-mHz sinusoidal waveforms and a load ratio of 0.2. All tests were carried out using the same loads and test practice, although the tests were conducted individually in a single-specimen autoclave. Macrophotographs of the specimens can be seen in Fig. 17, which shows that the crack fronts in these specimens are somewhat "fingered," indicating a high degree of nonuniformity in local growth rates along the crack front.

The effects of crack plane orientation on crack growth rates in A 516 can be seen in Figs. 18 and 19. The main feature of these results is that a great deal of variability can be realized, even for identical orientations of specimens. Specimens FOK-30 and FOK-32 were cut from neighboring locations in the parent plate, yet exhibit a factor of three difference in growth rates. Specimen FOK-30 exhibits a substantial variability in growth rates by itself. Comparison of the results for specimen FOK-34 in Fig. 19a with specimen FOK-33, in Fig. 9, two specimens of the same orientation, shows that the 1-Hz data sets exhibit the same rates in both cases, although there is a definite non-linearity in the trend of the data for specimen FOK-34. This bending-over may be microstructurally induced, and this change in microstructure may also result in the relative lack of environmental assistance for the 17-mHz part of the test. Comparison of the 17-mHz results from FOK-34 with the 1-Hz results from FOK-33 reveals one of

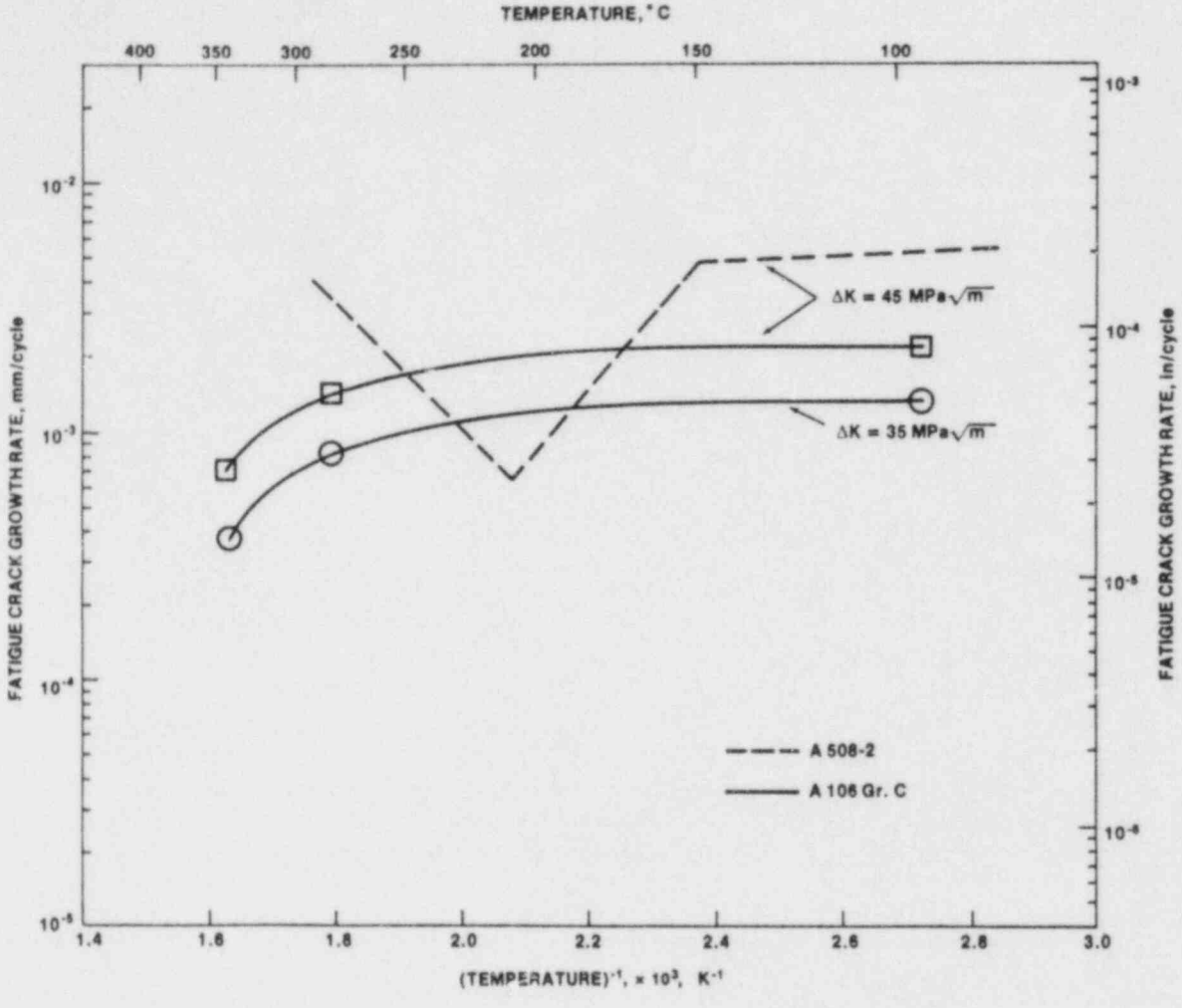

Fig. 16 Fatigue crack growth rates vs. inverse temperature, for applied cyclic ΔK's of 35 and 45 MPa$\sqrt{m}$ for A 106 Gr. C steel, at a test frequency of 17 mHz, and a load ratio of 0.2.

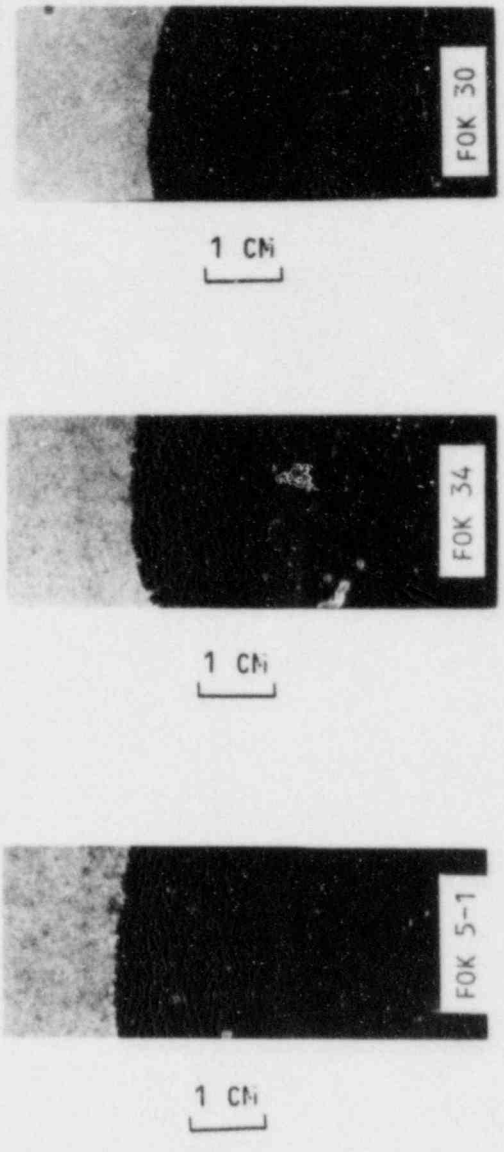

Fig. 17 Macrophotographs of test specimens of A 516 Gr. 70 steel for three orientations. Note the irregular crack front, due to the strong influence of the microstructure and manganese sulfide phase morphology, as discussed below.

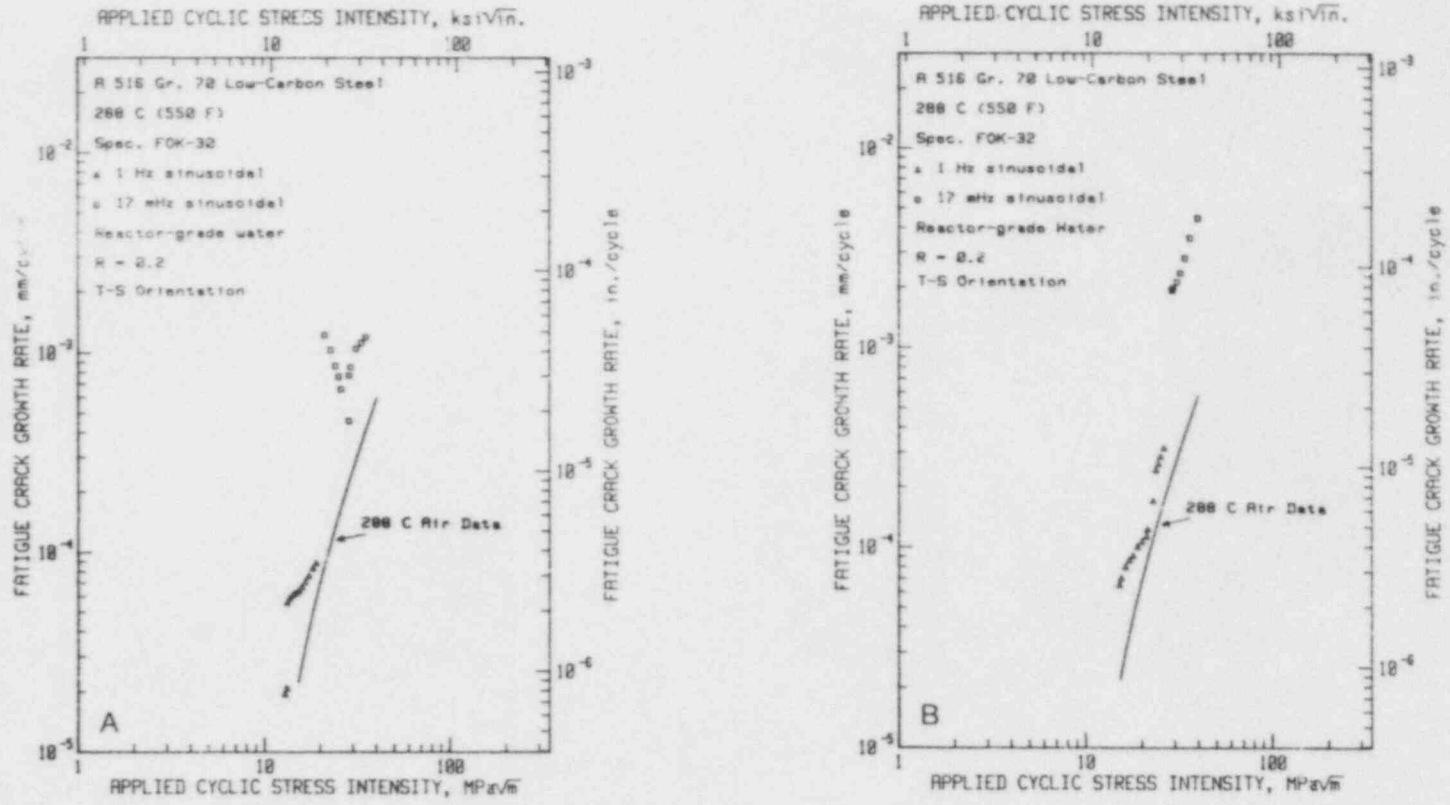

Fig. 18 Fatigue crack growth rates vs. applied cyclic ΔK for two specimens of steel in 288°C PWR environment for test frequencies of 1 Hz and 17 mHz, in the S-T orientation. Note the high degree of variability in crack growth rates, both within specimen FOK-30 (a) by itself, and between the two specimens, due again to the microstructural variability.

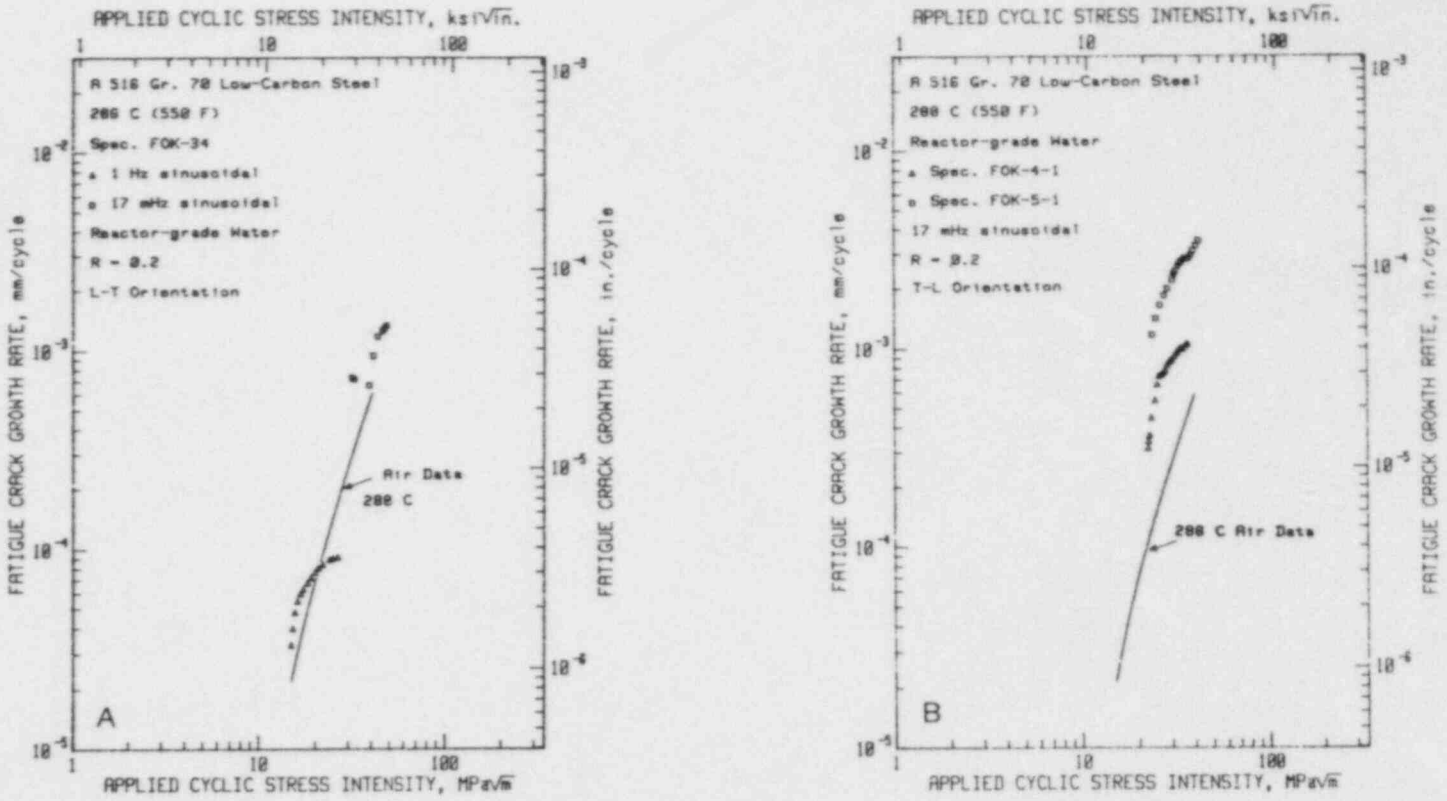

Fig. 19 Fatigue crack growth rates vs. applied cyclic ΔK for two orientations of A 516 Gr. 70 steel in 288°C PWR environment for a load ratio of 0.2. As in Fig. 18, there is considerable variability in these growth rates.

the few instances in which 1-Hz results exhibit faster growth rates than 17-mHz results for a load ratio of 0.2, and is again testimony to the way in which microstructures can influence the growth rates. This effect is exacerbated by the use of 1T specimens for cases where a plate product is being investigated, as was the case for this orientation study. Any large variations in the microstructure, such as large sulfide inclusions, carry significantly more influence in the smaller specimen than they would in a 2T specimen. Lastly, Fig. 19b shows data sets for the T-L orientation, an orientation which generally exhibits the fastest growth rates, or the lowest fracture energies, because the manganese sulfide inclusions, and the grain structure in general is oriented to result in somewhat easier separation. This case also is an example of the variability which is possible, although the average growth rate from the two specimens is somewhat faster than those for other orientations. Tests of both specimens FOK-4-1 and FOK-5-1 were fraught with experimental difficulties related to maintaining an accurate LVDT response. This necessitated opening the autoclave several times during the course of the tests, and then restarting the tests using the customary start-up procedures described above.

3.1.4 Metallographic and Fractographic Studies of Orientation Effects in A 516

In order to substantiate some of the effects observed in the fatigue crack growth rate data from the orientation-effects study on A 516, a metallographic and fractographic study was carried out. Polished and etched metallographic sections are shown in Fig. 20. The manganese sulfide (MnS) inclusions are clearly elongated in the L-direction, and have an aspect ratio of about unity in the L-plane (i.e., the S- and T-directions) Sulfur prints of the specimens, taken from a plane of about 1 or 2 mm under the fracture surface (Fig. 21) show that the density of inclusions cut by the crack in the S-T orientation (specimens FOK-30 and FOK-32) is much lower than for the other specimens. This fact alone does not bear a one-to-one relationship to the growth rates, since growth rates were high for these two specimens. Fracture profiles from the specimens, shown in Fig. 22, indicate that the fracture plane is rather smooth at low ΔK values (e.g., $\Delta K \sim 20$ to 22 $MPa\sqrt{m}$), but becomes quite rough and irregular at the higher ΔK values, towards the end of the test. This seems to be related to an increased amount of microcracking associated with the inclusions at various levels above and below the nominal fracture plane.

Before examination in the scanning electron microscope (SEM), the specimens were cleaned in acetone and the high-temperature oxide was removed with an ENDOX treatment (Ref. 30). In the fractographs shown below, there is one dominant trend. In regions where the growth rates were increased by environmental assistance, the fatigue fracture surface is brittle-like. When the growth rates were relatively unaffected by the environment, the surface is more ductile in character. The brittle-like regions can often be associated with the presence of manganese sulfide inclusions on the fatigue fracture surface.

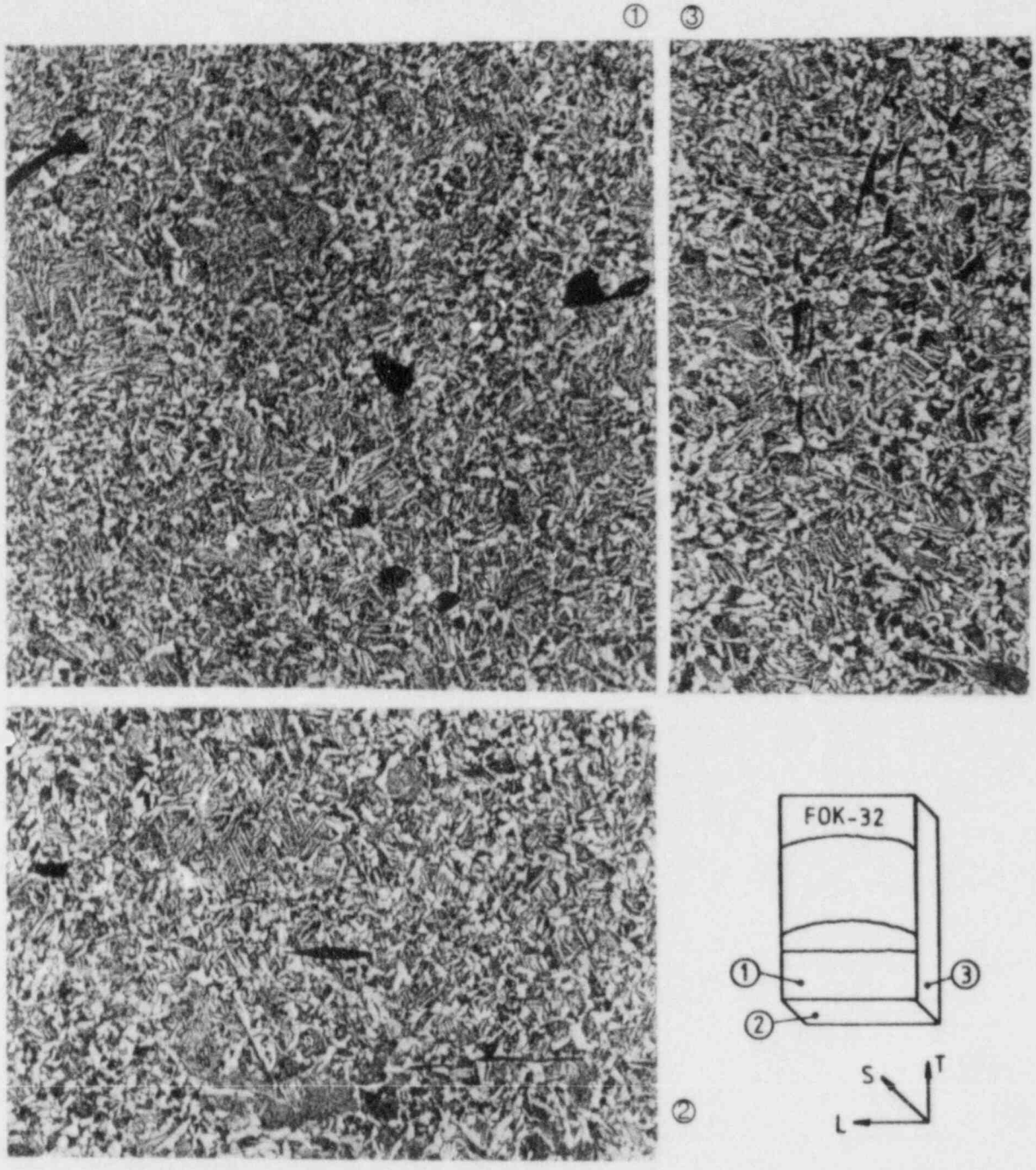

Fig. 20 A three-plane view of the microstructure of the A 516 Gr. 70 low-carbon steel investigated in this research. Note the aspect ratio of roughly unity on the S-plane (#1), and the elongated inclusion profiles on the T- and L-planes (#2 and #3).

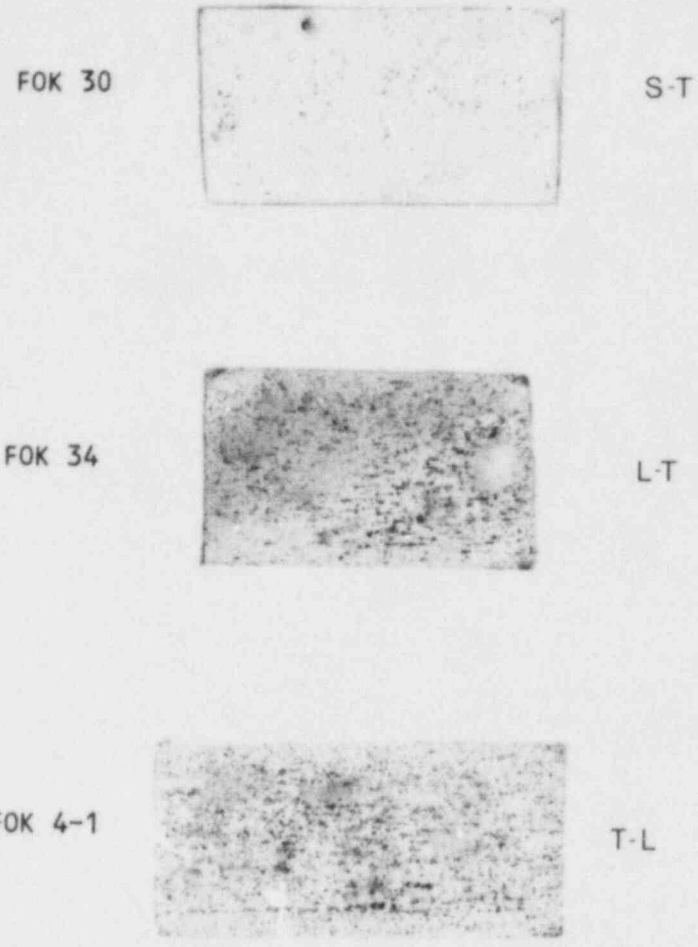

Fig. 21 Sulfur prints of specimens from the three orientations of A 516 Gr. 70 studied for this report. These prints were taken from a plane about 1 mm below the fatigue fracture. In each case, the crack moved from left to right. Note the apparent low density in specimen FOK-30 is a consequence of the fact that the inclusions have their elongated axis pointing out of the page.

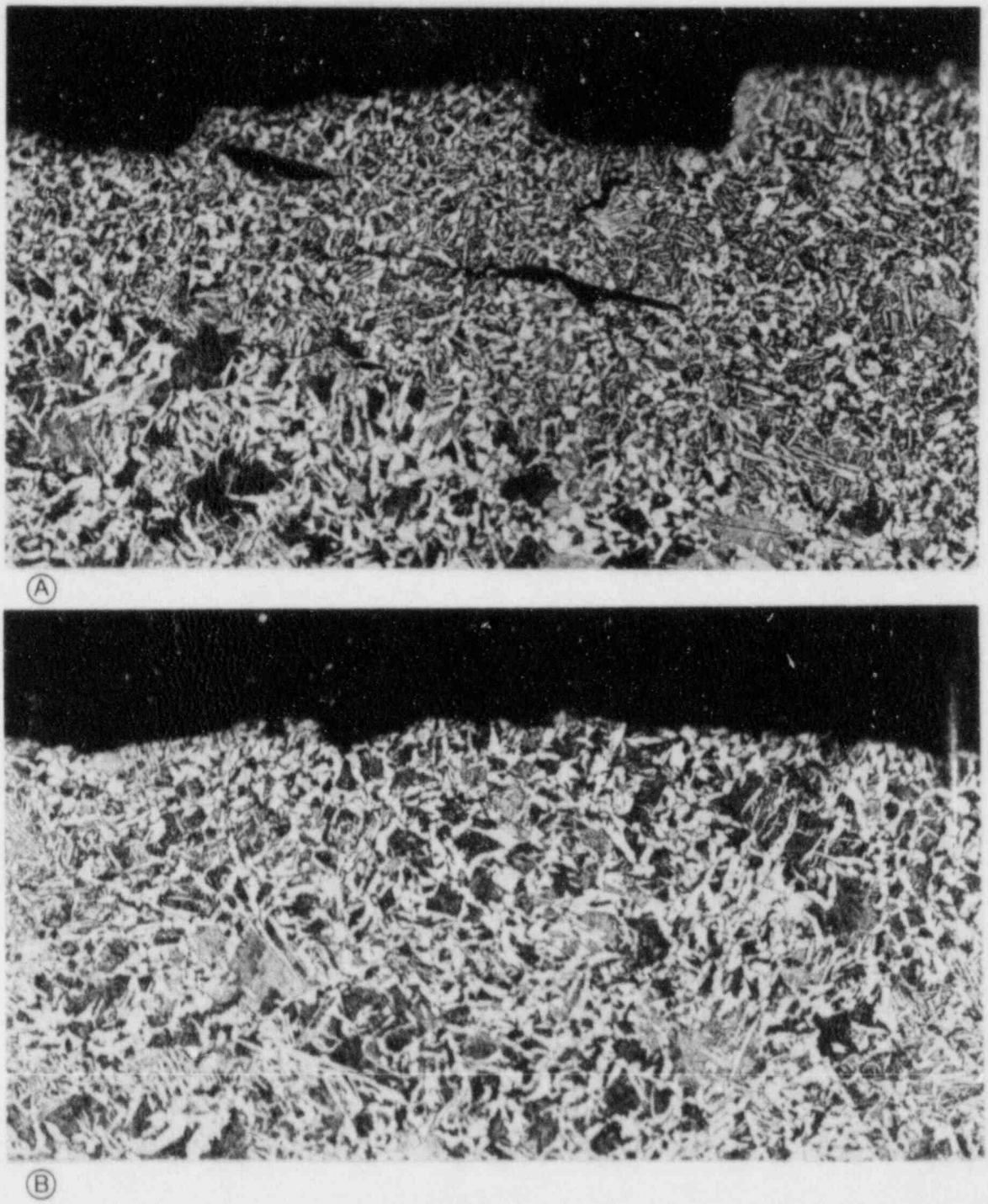

Fig. 22 Metallographic sections orthogonal to the fatigue fracture plane for two levels of ΔK: (a) 22 MPa$\sqrt{m}$, and (b) 26.5 MPa$\sqrt{m}$. Note the irregular surface of the crack plane at the higher ΔK value, and the greater occurrence of microcracks below the fatigue fracture surface. Such cracks generally indicate a hydrogen-assisted crack extension mechanism, since the environment has no direct access to these cracks.

Illustrations of these features are shown in Figs. 23 to 31. Even in the portion of the fatigue crack opened at 1 Hz, brittle-like features are seen to emanate from the regions formerly containing manganese sulfide inclusions, as shown in Fig. 23. This figure can be compared with Fig. 24, taken from the 17-mHz part of the test on the same specimen, to see that the two areas are remarkably similar in appearance. There is, however, a much greater degree of microcracking to be seen at the higher ΔK. Nearly all the fatigue fracture surfaces of this series of specimens are covered with fan-shaped features. Superimposed on these fan-shaped features may be either ductile or brittle striations. Examples of ductile striations can be seen in Fig. 25, and examples of brittle striations can be seen in Fig. 26.

An example of the local variation along the crack front is shown in Fig. 27, along with the accompanying schematic in Fig. 28. The manganese sulfide inclusion has provided apparently a route for rapid advancement of the crack front. This may occur because of the relatively low energy required to break the inclusion, or to separate it from the matrix. At that point, the environment is free to invade more deeply, and environmentally-assisted crack growth radiates from the manganese sulfide stringers as shown in Fig. 29. Evidence of a similar event is shown in Fig. 30, in which an inclusion is surrounded completely by brittle-like, fan-shaped features, indicating the apparently high degree of chemical influence caused by the reaction of the environment with the dissolving sulfide particle. Figure 30 also shows a high degree of microcracking in the region surrounding the MnS particles. The microcracking is usually more visible at the high ΔK values. Both the brittle-like features (including the brittle striations, and the fan-shaped features) and the microcracking are often associated with hydrogen-assisted crack growth. Note that in Figs. 23, 24 and 27, all taken from specimens in the S-T orientation, the manganese sulfide inclusions are elongated from right to left, which is the rolling direction. Figure 31 is taken from the fatigue fracture surface of FOK-4-1, in the T-L orientation, and shows the same degree of fan-shaped features and microcracking as the other micrographs. In this case however, the traces of the MnS inclusions are very thin and oriented in the L-direction, parallel to the direction of crack extension.

Although the series of micrographs is too extensive to be shown here, examination of specimen FOK-30, which exhibited a "V"-shaped da/dN vs. ΔK trend curve, showed that the growth rates could be related directly to the density of MnS inclusions on the fatigue fracture surface. Where growth rates were high, at the beginning and end of the 17-mHz portion of the test, the inclusion density was also high.

3.2 Load Ratio and Temperature Effects in SA 351-CF8A Cast Stainless Steel

Tests were carried out on specimens of cast stainless steel to evaluate the response of fatigue crack growth rates to a range of load ratios and temperatures. The complete results of the investigation of temperature dependence are contained in an earlier report (Ref. 20); the results below are a only summary. Figure 32 shows crack growth

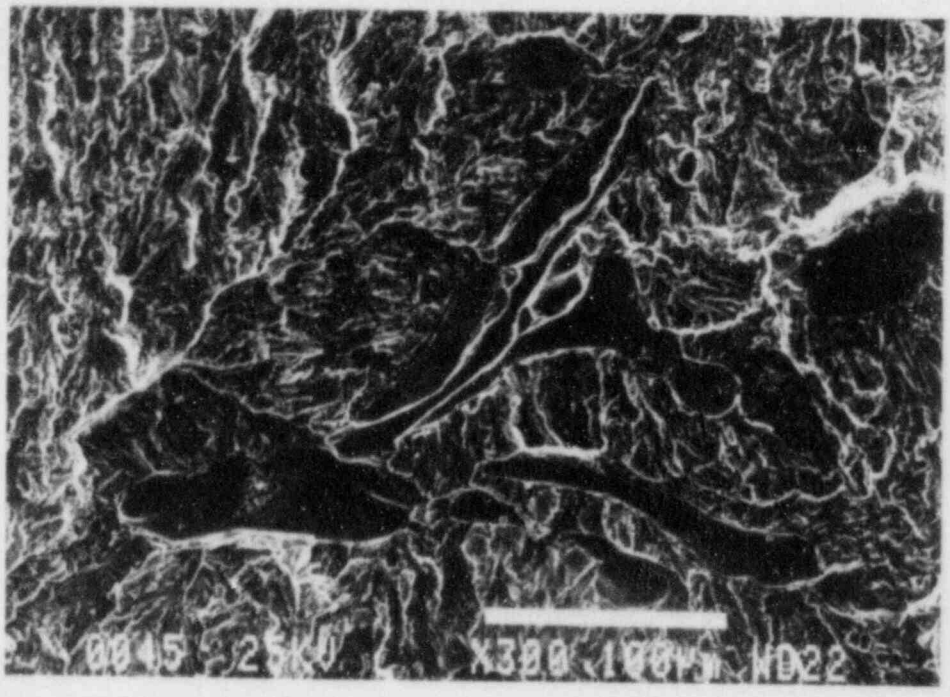

Fig. 23 Fatigue fracture surface showing the brittle-like, fan-shaped features develcped at 1 Hz test frequency. Specimen is FOK-30, ΔK = 15 MPa$\sqrt{m}$.

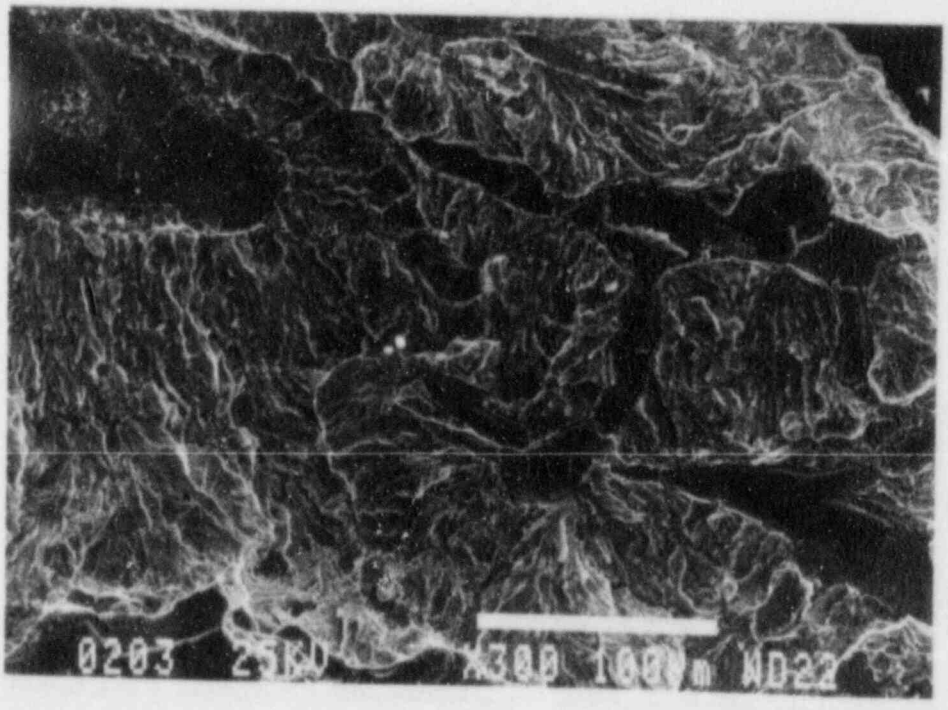

Fig. 24 Fatigue fracture surface showing the brittle-like, fan-shaped features developed at 17-mHz test frequency. Specimen is FOK-30, ΔK = 27 MPa$\sqrt{m}$.

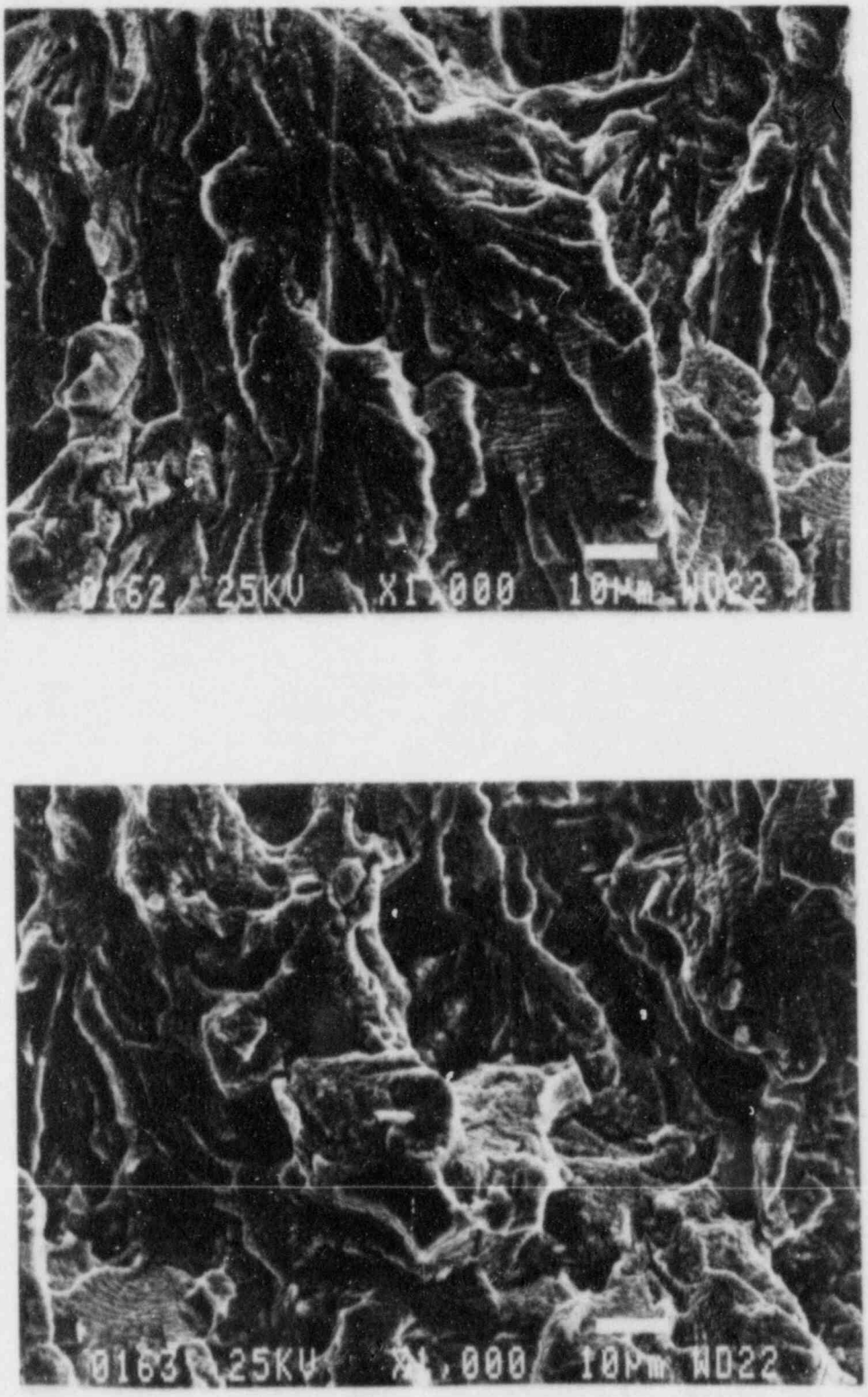

Fig. 25 An example of the ductile striations which may be found superposed on the fan-shaped features. Specimen is FOK-5-1, ΔK = 21 MPa$\sqrt{m}$.

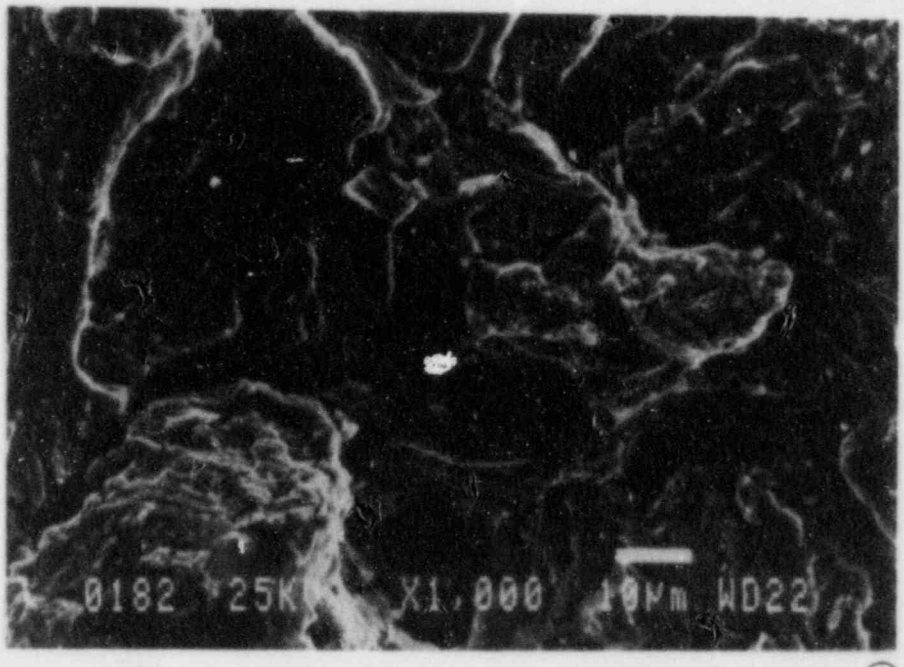

Ⓐ

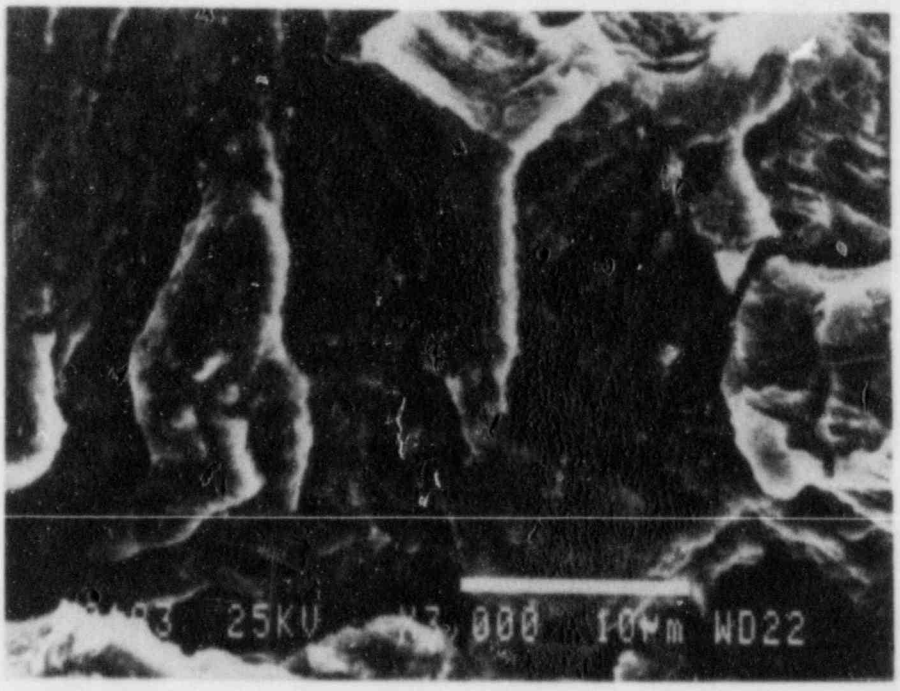

Ⓑ

Fig. 26 An example of the brittle striations which may be found superposed on the fan-shaped features. Specimen is FOK-5-1, ΔK = 30 MPa$\sqrt{m}$.

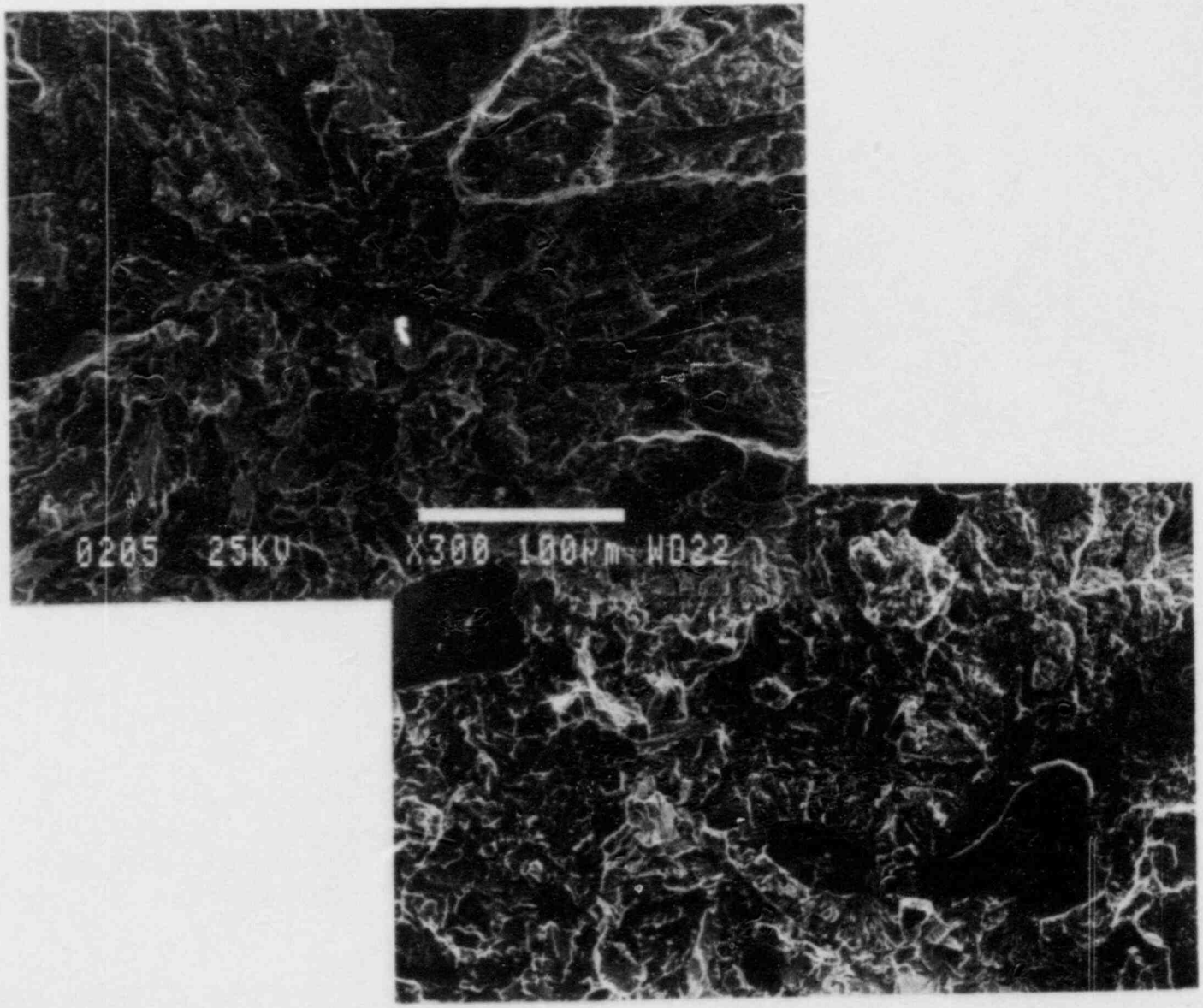

Fig. 27 An SEM micrograph showing the variation along the crack front, due to influence of manganese sulfide inclusions on environmentally-assisted crack advance. Note that the fatigue crack has spread out in all directions from the tip of the manganese sulfide inclusion. Specimen is FOK-30, ΔK = 34 MPa$\sqrt{m}$.

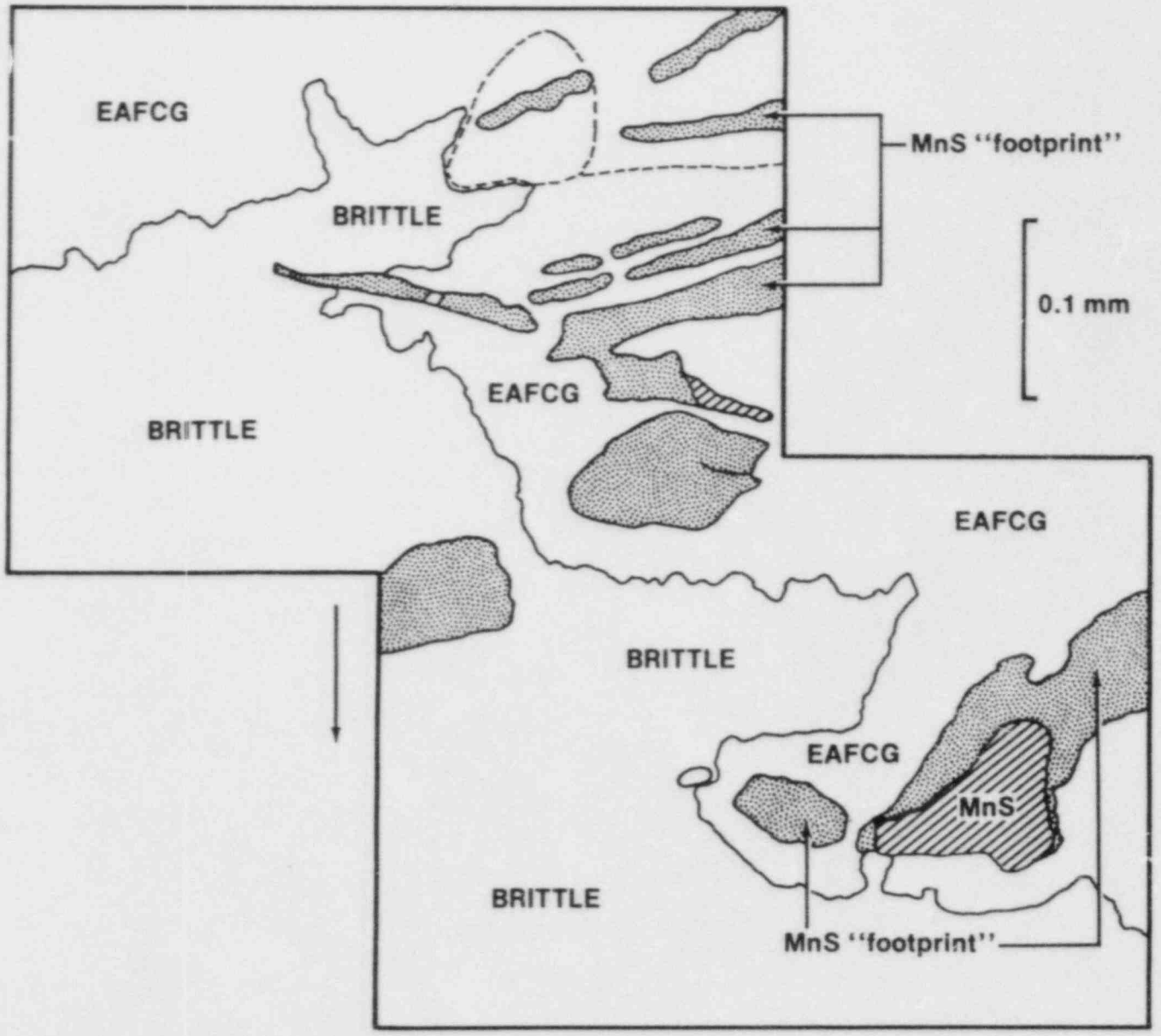

Fig. 28 A schematic accompanying the micrograph shown in Fig. 27, and identifying the various areas and types of fracture.

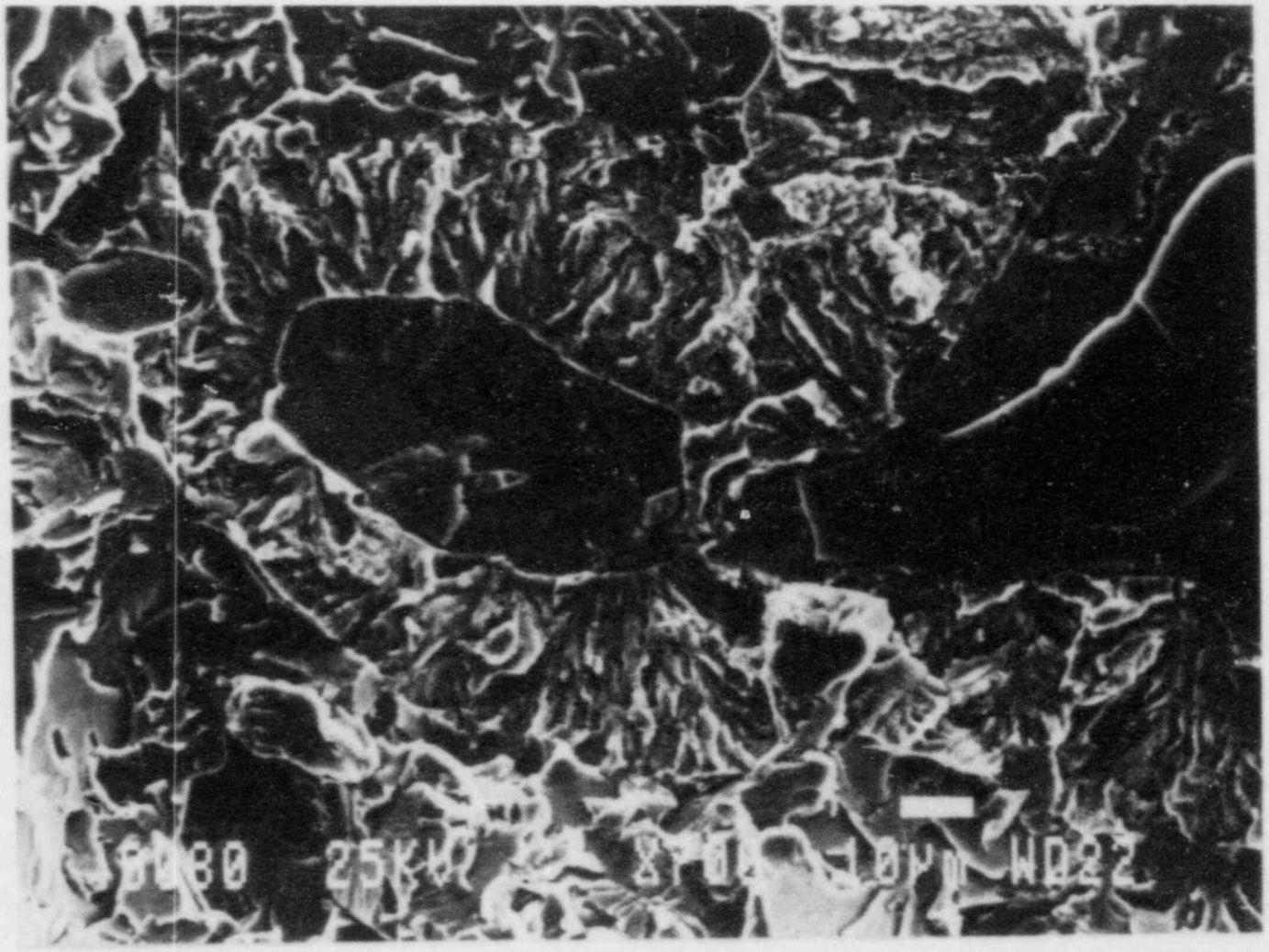

Fig. 29 An enlargement of Fig. 27 showing the way in which environmentally-assisted crack growth emanates from the boundaries of the manganese sulfide inclusions.

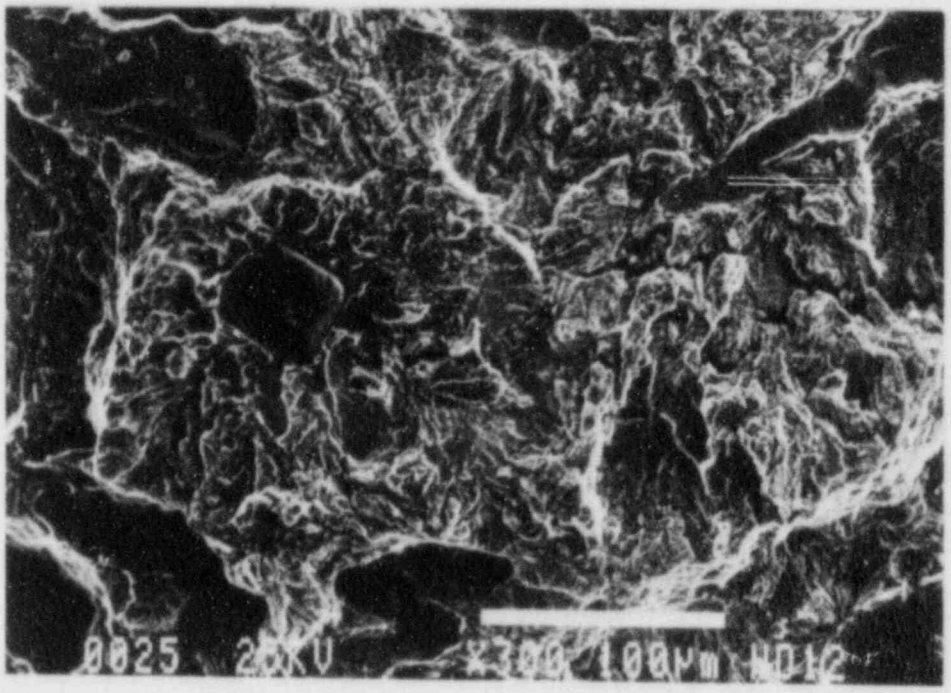

Ⓐ

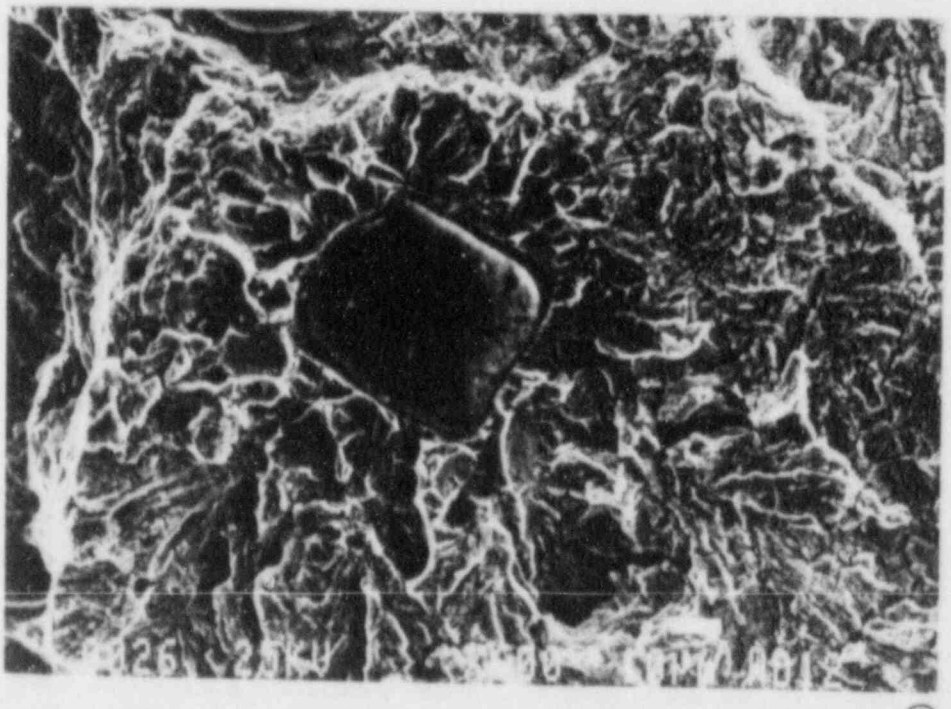

Ⓑ

Fig. 30 SEM micrographs of a manganese sulfide inclusion completely surrounded by brittle-like fracture. Features such as this, which must have occurred ahead of the location of the crack tip, suggest that hydrogen might have assisted the fracture. Specimen is FOK-32, ΔK = 48 MPa$\sqrt{m}$. Fig. 30b is an enlargement of Fig. 30a.

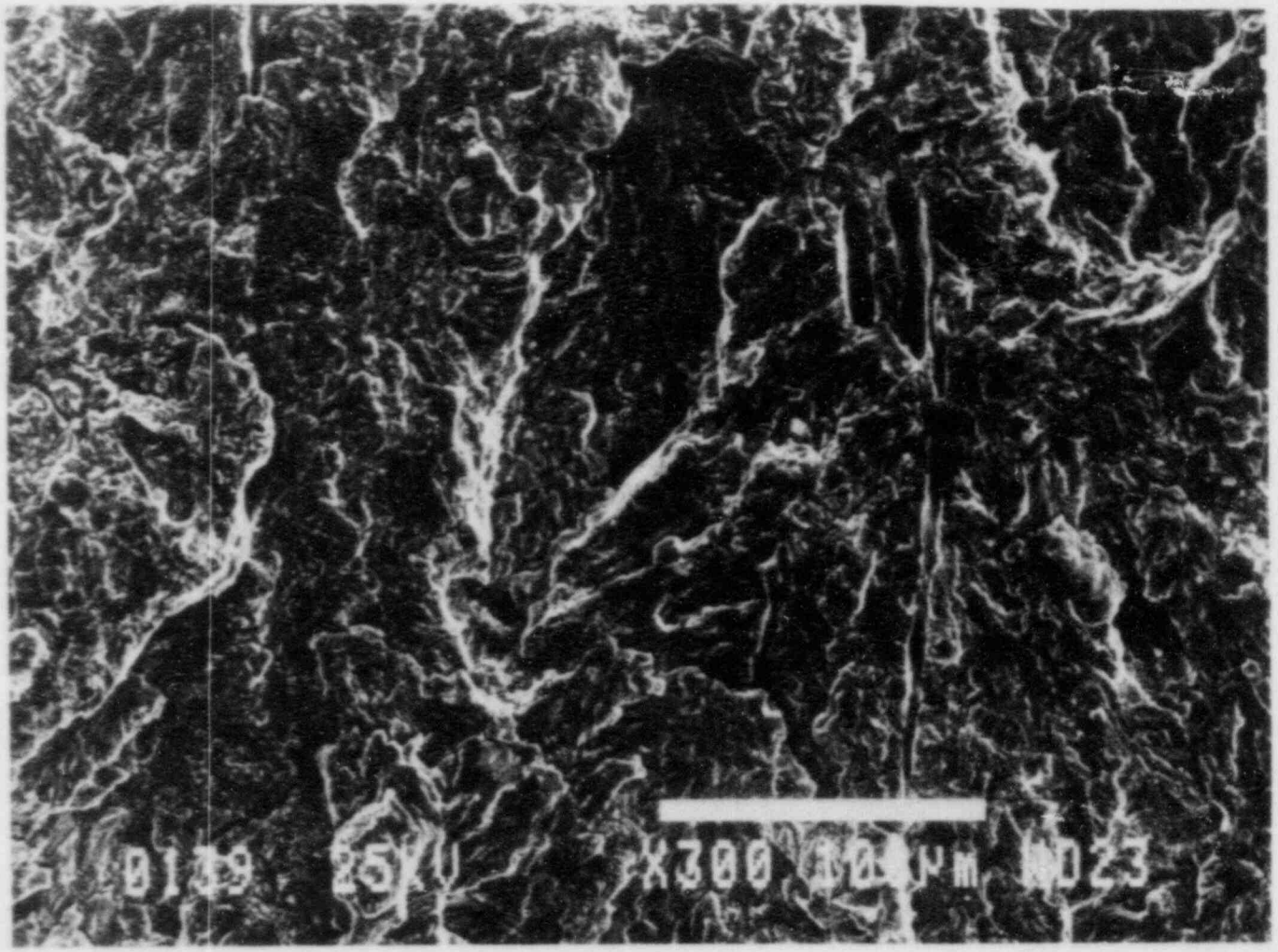

Fig. 31 Fatigue fracture surface from specimen FOK-4-1, in the T-L orientation at ΔK = 35 MPa$\sqrt{m}$. showing that the trace of the manganese sulfide inclusion has a very high aspect ratio, and that the spread of fan-shaped features from the site of the inclusion is not as pronounced as for the S-T orientation.

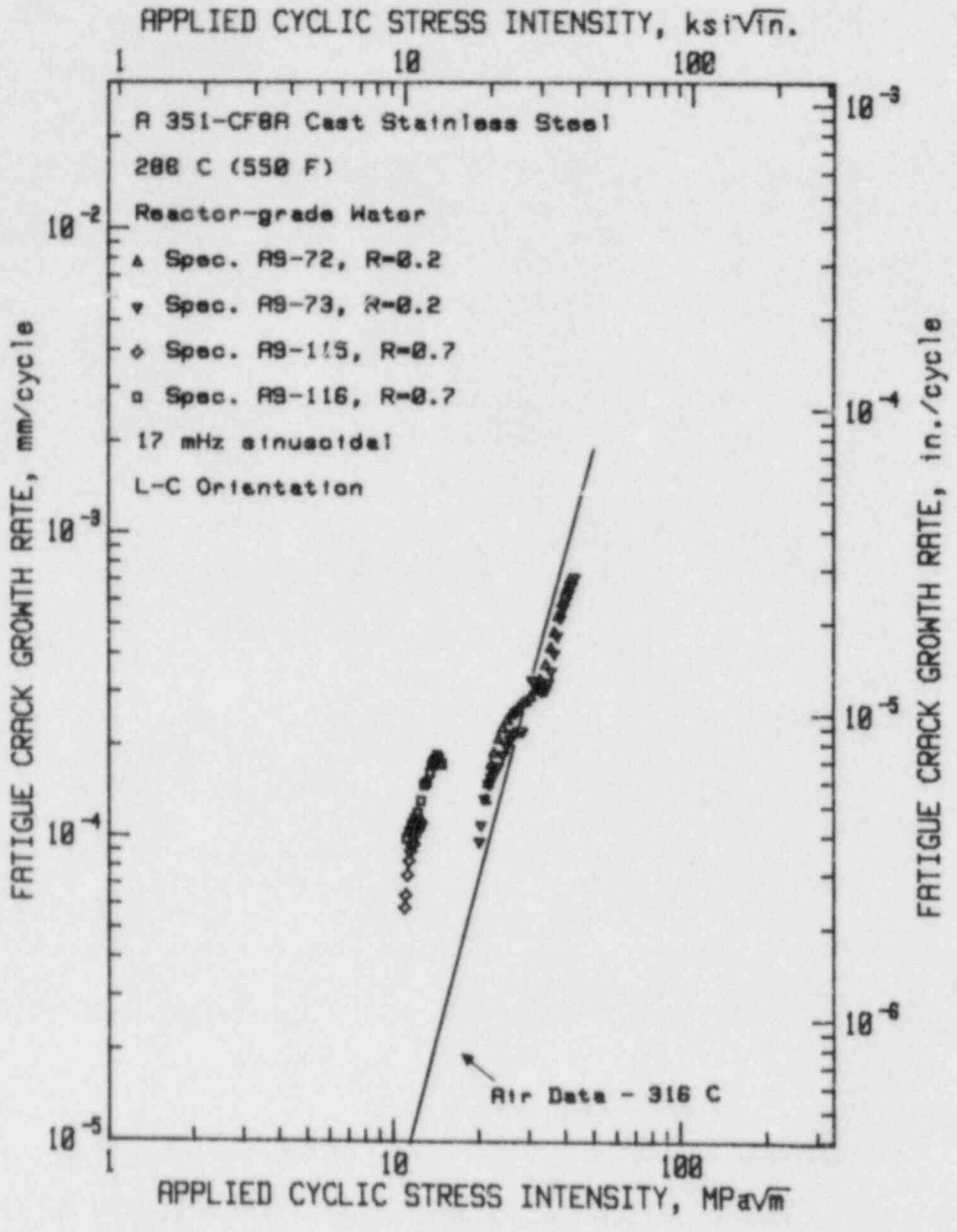

Fig. 32 Fatigue crack growth rates vs. applied cyclic stress intensity factor for A 351-CF8A for load ratios of 0.2 and 0.7, 17-mHz test frequency and a temperature of 288°C.

rate results for load ratios of 0.2 and 0.7. The growth rates for the 0.7 case show the customary increase, as compared on a ΔK basis with the growth rates for the 0.2 cases. However, they show about the same slope, or dependence on ΔK, as do the 0.2 results in high-temperature water. The air test was conducted using a 1T-CT specimen, hence the abbreviated ΔK range as compared with the aqueous environment tests, all carried out with 2T-CT specimens, which support a higher maximum applied ΔK. Many of the appropriate figures also include a trend line which represents a large volume of data for air environment tests, mostly taken from references by James (Refs. 31-32).

Figures 33 to 35 show fatigue crack growth rates for two orientations of the cast stainless specimens at temperatures of 232°C, 288°C and 338°C (450°F, 550°F and 650°F), all at a load ratio of 0.2. On Fig. 35, the data for the highest temperature, trend lines for the 232°C and 288°C data are also shown. It is easily seen that the growth rates at 338°C are considerably higher than growth rates at the other two temperatures. Even though only one test of two specimens was conducted confidence in the accuracy of this data seems assured, because of the evidence from the multispecimen test cited in Section 3.1.2. It is interesting to note the roughly sigmoidal shape of the growth rate curves at the temperatures of 232°C and 288°C, indicating that there is a higher proportion of environmental assistance at the lower range of ΔK than at the higher range.

Figures 36 to 39 show SEM micrographs of the fatigue fracture surfaces of specimen A9-70, tested at 288°C. This fractographic examination showed that the main characteristic was the brittle appearance. This behavior is similar to that of the low-alloy steels, but even more similar to the morphology found on stress-corrosion cracking surfaces of stainless steel specimens which have been sensitized (although these were not) or which are tested in very aggressive environments (Ref. 33). In Fig. 36, the reader should note the fan-shaped features, and brittle-appearing morphology which cover the fatigue fracture surface. Many of these fan-shaped features have other markings, such as striations and slip lines. An extensive investigation showed that there were three basic combinations of features in which striations could be found. These are shown in Fig. 37. The top panel in this figure shows a high magnification view of brittle-like striations found on one of the fan-shaped features. The middle panel shows ductile striations on a fan-shaped feature, and the bottom panel shows fully ductile striations found on transgranular fatigue fracture surfaces. Another unique feature found within the brittle-appearing regions is the presence of slip lines which have intersected the surface. These are especially visible in the SEM because they appear to be "decorated" with oxide. Examples of these characteristics are shown in Fig. 38.

Figure 39 shows the way in which the crack front intersects the delta-ferrite phase boundaries with little or no perturbation. Even the river pattern established in the leading fan in the austenitic phase is carried through the delta-ferrite and continues into the austenite on the other side. In many, if not most cases, the delta-ferrite-austenite boundary is cracked, normal to the fatigue crack, always on

Fig. 33 Fatigue crack growth rates vs. applied cyclic stress intensity factor for A 351-CF8A for a load ratio of 0.2, 17-mHz test frequency, and a temperature of 232 °C.

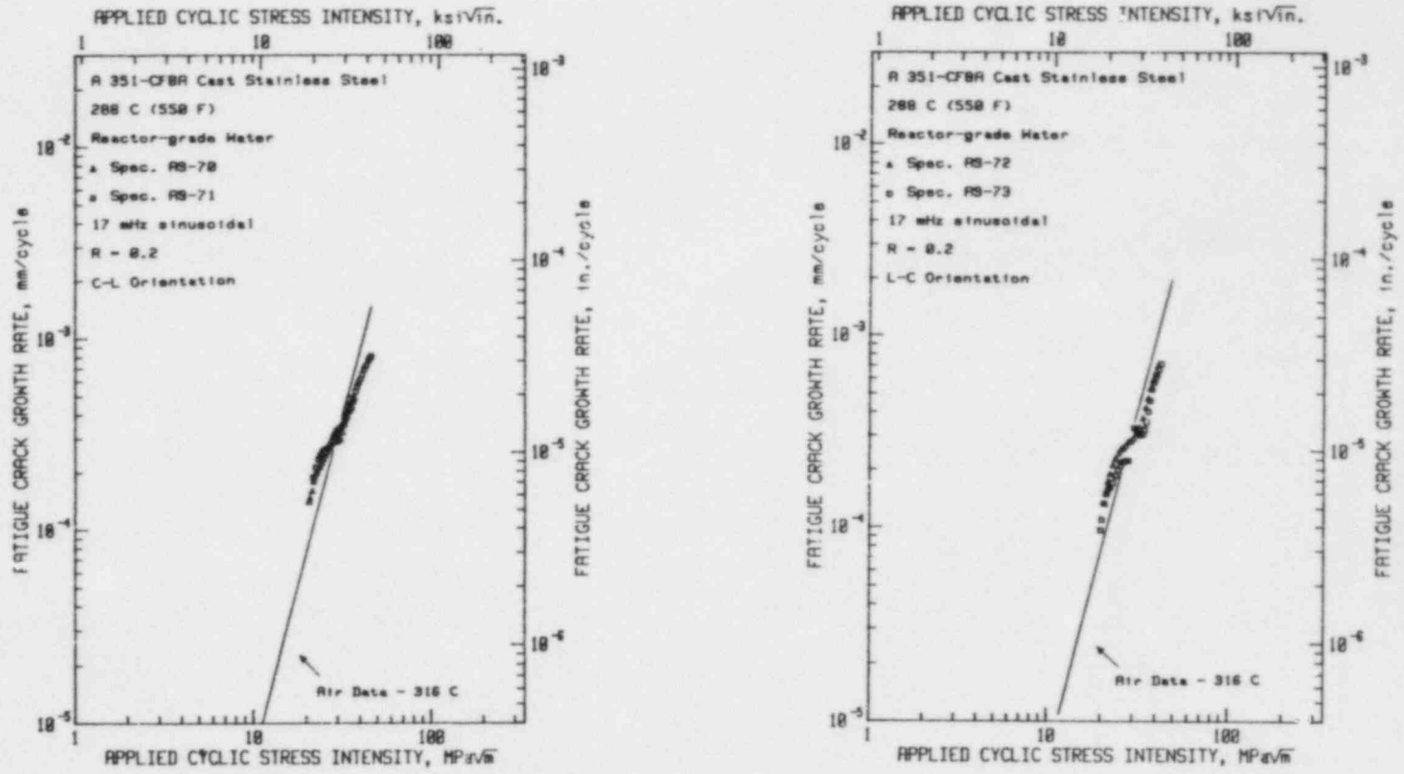

Fig. 34 Fatigue crack growth rates vs. applied cyclic stress intensity factor for A 351-CF8A for a load ratio of 0.2, 17-mHz test frequency, and a temperature of 288°C.

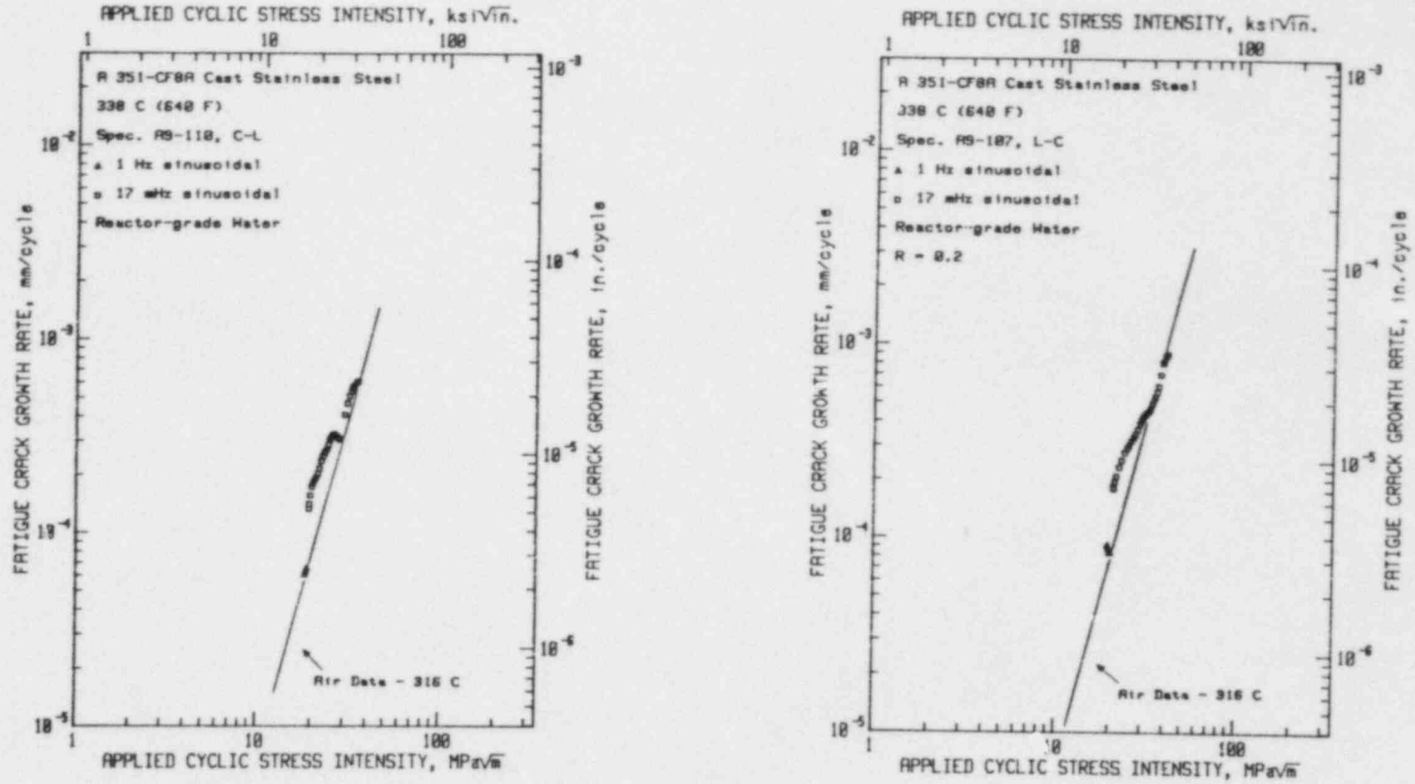

Fig. 35 Fatigue crack growth rates vs. applied cyclic stress intensity factor for A 351-CF8A for a load ratio of 0.2, 17-mHz test frequency, and a temperature of 338°C. These data sets are also shown in Fig. 15.

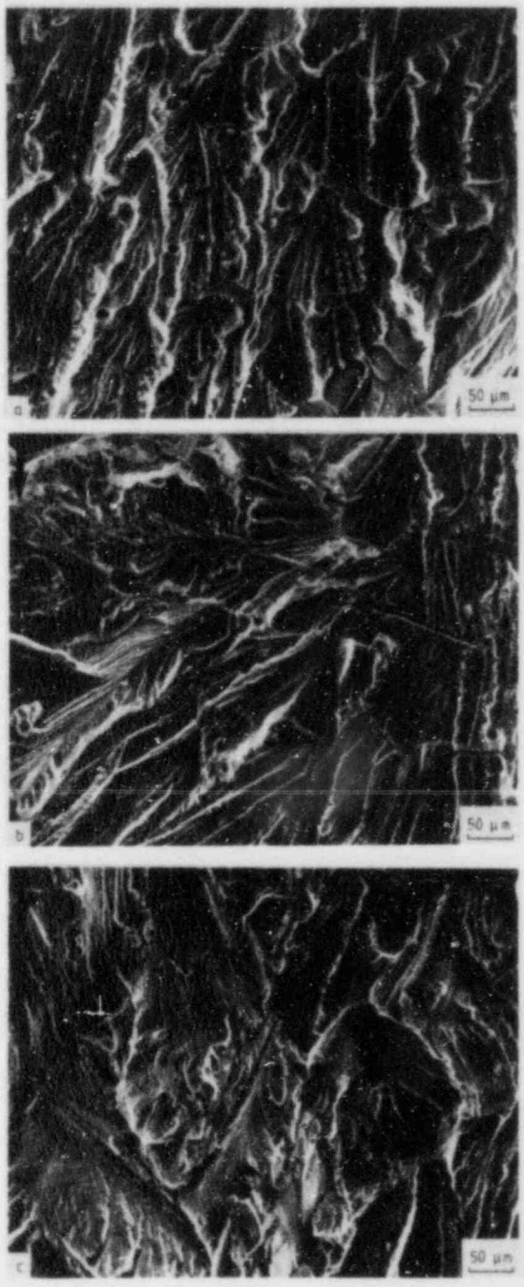

Fig. 36 Fractographic features of environmentally-assisted fatigue crack growth in A 351-CF8A cast stainless steel. ΔK = 25 MPa$\sqrt{m}$ in (a) and (b); ΔK = 20 MPa$\sqrt{m}$ in (c). Test temperature was 288°C. Note the fan-shaped features and overall brittle appearance.

Fig. 37 Fractographic features of environmentally-assisted fatigue crack growth in A 351-CF8A cast stainless steel. $\Delta K = 30$ MPa$\sqrt{m}$. Test temperature was 288°C. Brittle striations are shown in (a); ductile striations on a fan-shaped feature in (b) and fully ductile striations in (c).

Fig. 38 Fractographic features of environmentally-assisted fatigue crack growth in A 351-CF8A cast stainless steel. $\Delta K = \sim 20$ MPa$\sqrt{m}$. Test temperature was 288°C. The linear features are slip steps which have been "decorated" with oxide.

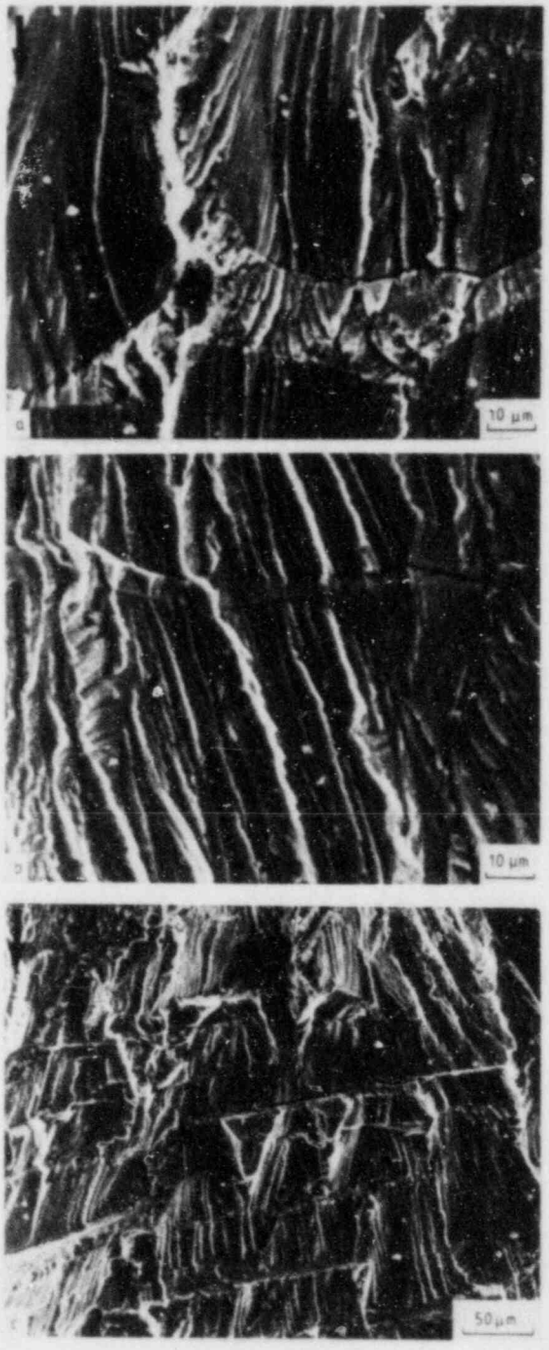

Fig. 39 Fractographic features of environmentally-assisted fatigue crack growth in A 351-CF8A cast stainless steel. $\Delta K = \sim 20$ MPa$\sqrt{m}$ in (a) and (b), 25 MPa$\sqrt{m}$ in (c). Test temperature was 288°C. These three panels show the morphology developed when the fatigue crack cuts through the delta-ferrite phase. Note that the austenite ferrite boundary is cracked on the edge first intercepted by the crack, never on the trailing edge.

the first of the pair of boundaries to be intersected by the crack. A more complete description of these observations is contained in Reference 34.

Figure 40 shows a plot of all the data sets on stainless steel presented in this report, along with upper bound lines suggested by Slama (Ref. 15). It can be seen that for the most part these data sets, all for R = 0.2 or less, fall within the suggested bounds, which also include the data published previously by Bamford. Altogether, there are now published results from tests of over fifty specimens at three laboratories; all reside within these bounds, which are somewhat lower in da/dN vs. ΔK than the reference lines from the ASME Code for pressure vessel steels.

4.0 SUMMARY AND CONCLUSIONS

This section is divided into summary and conclusion sets for the carbon steels, and for the stainless steels.

4.1 Carbon Piping Steels, A 106 Gr. C and A 516 Gr. 70

Fatigue crack growth rate tests in PWR environments have been carried out for these steels under a variety of test frequency, temperature and load ratio conditions. Many combinations of these critical variables produced significant components of environmental assistance. The microstructure of these steels, particularly the manganese sulfide inc sions, played a major role in the progress of the fatigue crack. There can be considerable variability in fatigue crack growth rates for some steels, as shown in the A 516 in Figs. 18 and 19. The increase in growth rates as a function of ΔK with an increase in load ratio is in line with the increase observed in pressure vessel steels. The temperature dependence of crack growth rates in A 106 is different in form from that of A 508-2 pressure vessel steel, but covers basically the same extremes.

The conclusions are as follows:

(1) Crack growth rates in these steels are of the same order of magnitude, and exhibit the same basic dependence on the known critical variables as those of pressure vessel steels.

(2) The frequency dependence of crack growth rates seems to be tied to the load ratio, with 1-Hz test frequencies often resulting in higher growth rates than 17 mHz at the higher load ratios.

(3) The manganese sulfide inclusions play a major role in the crack plane morphology and in the crack growth rates. In a study with a limited sampling of steels such as this one, it is impossible to predict an upper limit which might occur because of a detrimentally high concentration of sulfide inclusions; but clearly, from the results in Figs. 18a and 19b, rather high growth rates are possible.

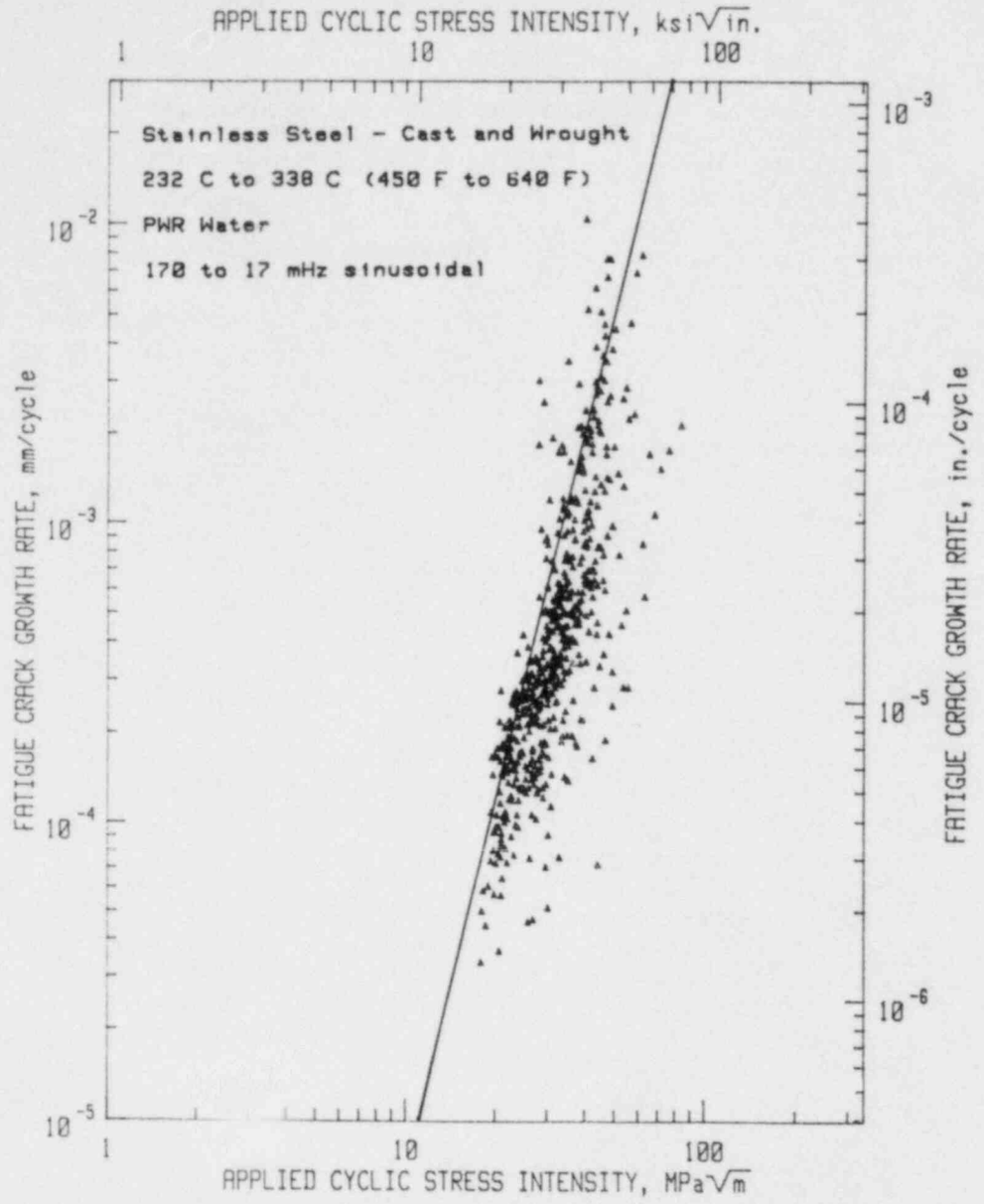

Fig. 40 Fatigue crack growth rates vs. applied cyclic stress intensity factor for stainless steel data sets in this report and those referenced previously (Refs. 12 and 15). The upper bound lines have been suggested by Slama (Ref. 15).

(4) Many features of the fractography of the A 516 specimens suggest that the crack growth rates are affected by a hydrogen-assistance mechanism.

4.2 Cast Stainless Steel, A 351-CF8A

Crack growth rates in the stainless steels lie within the same range as the carbon steels described above, but the dependencies on the critical variables are somewhat different. Crack growth rates at 1 Hz show usually less environmental assistance than at 17 mHz, for load ratios of both 0.2 and 0.7, although the data base at 0.7 suffers from its content of only two tests. The temperature dependence of crack growth rates shows that rates increase as the temperature increases. The fatigue fracture surface morphology shows brittle-like features cover nearly all of the fracture surface, and that the crack progress is not influenced by the delta-ferrite phase.

The conclusions are as follows:

(1) The amount of environmental assistance provided to the fatigue crack growth rates may be directly proportional to the test frequency, and is basically independent of the load ratio. Growth rates at 232°C and 288°C showed relatively little environmental component.

(2) The temperature dependence of crack growth rates shows a modest increase in growth rates with increase in temperature, for load ratios of 0.2.

(3) Fractographic features show that regions of ductility can abut regions of highly brittle-like fatigue striation formation, suggesting that crack growth rates do not depend directly on the mechanics of crack tip deformation. Overall, brittle-like features cover nearly all of the fatigue fracture surface.

5.0 FUTURE RESEARCH NEEDS

This study, together with some of the references cited in the text, represents the beginning of the accumulation of a data base for fatigue crack growth rates for piping steels in LWR environments. Through these studies, some of the influence of a few key critical variables is beginning to be understood. Some of the areas which should be covered in future research projects are as follows:

For the carbon steels:

(1) The frequency dependence of fatigue crack growth rates, and its interaction with load ratio, needs to be clarified. There are indications that high test frequencies, together with high load ratios, such as 10 Hz at R = 0.9, may provide high growth rates on a da/dN basis. Such a test is feasible from a laboratory test time and equipment standpoint.

(2) The influence of sulfide inclusions on crack growth rates needs to be studied in great depth, from either the macro- or micro-approach. That is to say, "worst-case" steels should be tested to determine the maximum increase in growth rates which might occur. Also, it would be interesting and potentially helpful to understand better the crack tip micromechanism through which the environment in the crack tip enclave is affected by the dissolving MnS inclusions, and the way in which the inclusions promote, if they do, increases in hydrogen-assisted crack growth.

For the cast stainless steels:

(1) Research is needed to define growth rates at the higher load ratios which are more typical of piping steels. The combination of high load ratios and high temperatures (typical of hot leg conditions) should be investigated.

(2) Since the fractographic features are essentially the same for fatigue crack growth and stress-corrosion cracking tests, the time dependence of crack growth rates should be determined. This can be accomplished by carrying out tests at lower test frequencies, together with a choice of other suitable critical variables, such as high load ratio and high temperature. These tests are feasible, but somewhat difficult from a laboratory point-of-view.

REFERENCES

1. W. H. Cullen, "Effects of Loading Rate, Waveform and Temperature on Fatigue Crack Growth Rates of RPV Steels," Aspects of Fracture Mechanics in Pressure Vessels and Piping, S. S. Palusamy and S. G. Sampath, eds., PVP-58, Amer. Soc. Mech. Engineers, New York, NY, 1982, pp. 303-312.

2. P. M. Scott, and A. E. Truswell, "Corrosion Fatigue Crack Growth in Reactor Pressure Vessel Steels in PWR Primary Water," Paper PVP-82-029, Proc. of ASME Pressure Vessels and Piping Conference, Orlando, FL, June 1982, Journal of Pressure Vessel Technology, Vol. 105(3), 1983, p. 245.

3. W. H. Bamford, "Environmental Cracking of Pressure Boundary Materials, and the Importance of Metallurgical Considerations" in Aspects of Fracture Mechanics in Pressure Vessels and Piping, S. S. Palusamy and S. G. Sampeth, eds., PVP-58, Amer. Soc. Mech. Engineers, New York, NY, 1982, pp. 209-228.

4. P. M. Scott, A. E. Truswell and S. G. Druce, "Corrosion Fatigue of Pressure Vessel Steels in PWR Environments -- Influence of Steel Sulfur Content," Corrosion, Vol. 40(7), 1984, pp. 350-357.

5. J. M. Barsom, "Effect of Cyclic Stress Form on Corrosion Fatigue Crack Propagation Below K_{Iscc} in a High Yield Strength Steel," Corrosion Fatigue: Chemistry, Mechanics and Microstructures NACE-2, O. Devereux, A. J. McEvily and R. W. Staehle, eds., National Association of Corrosion Engineers, 1972, pp. 424-433.

6. O. Vosikovsky, "Effects of Mechanical and Environmental Variables on Fatigue Crack Growth Rates in Steel -- A Summary of Work Done at CANMET," Canadian Metallurgical Quarterly, Vol. 19, 1980, pp. 87-97.

7. R. J. Selines and R. M. Pelloux, "Effect of Cyclic Stress Wave Form on Corrosion Fatigue Crack Propagation in Al-Zn-Mg Alloys," Metallurgical Transactions, Vol. 3, 1972, pp. 2525-2531.

8. D. B. Dawson and R. M. Pelloux, "Corrosion Fatigue Crack Growth in Titanium Alloys in Aqueous Environments," Metallurgical Transactions, Vol. 5, 1974, pp. 723-731.

9. O. Vosikovsky, W. R. Neill, D. A. Carlyle and A. Rivard, "The Effect of Sea Water Temperature on Corrosion Fatigue Crack Growth in Structural Steels," CANMET Physical Metallurgy Research Laboratories Report ERP/PMRL 83-27 (OP-J), Ottawa, Canada, April 1983.

10. W. H. Cullen and K. Torronen, "A Review of Fatigue Crack Growth of Pressure Vessel and Piping Steels in High-Temperature, Pressurized, Reactor-Grade Water," USNRC Report NUREG/CR-1576, NRL Memorandum Report 4298, Sept. 1980.

11. W. H. Cullen and F. J. Loss, "Interpretation of USA Results on Corrosion Fatigue of RPV Steels in Typical PWR Environments," Structural Integrity of Light Water Reactor Components, Applied Science Publishers, 1982, pp. 275-286.

12. W. H. Bamford, "Fatigue Crack Growth of Stainless Steel Piping in a Pressurized Water Reactor Environment," J. Pressure Vessel Tech., Vol. 101, 1979, pp. 73-79.

13. J. L. Bernard and G. S. Slama, "Fatigue Crack Growth Curve in Air Environment at 300°C for Stainless Steels," Nuclear Technology, Vol. 59, 1982, pp. 136-147.

14. C. Amzallag, G. Baudry and J. L. Bernard, "Effects of PWR Environment on the Fatigue Crack Growth of Different Stainless Steels and Inconel-Type Alloys," in Proceedings of the International Atomic Energy Agency Specialists' Meeting on Subcritical Crack Growth, Vol. 1, USNRC Conference Proceedings NUREG/CP-0044, 1983, pp. 163-194.

15. G. Slama, P. Petrequin and T. Mager, "Effect of Aging on Mechanical Properties of Austenitic Stainless Steel Castings and Welds," in Proceedings of Post-Conference Seminar #6: Assuring Structural Integrity of Steel Reactor Pressure Boundary Components, to be published, 1983.

16. D. A. Hale, "Materials Performance in a Startup Environment," a series of progress reports on EPRI Contract RP-1332-2 including GE Report NEDC-24392, Vol. 1, April 1982.

17. T. A. Prater, W. R. Catlin and L. F. Coffin, "Environmental Crack Growth Measurement Techniques," EPRI NP-2641, Nov. 1982.

18. T. A. Prater and L. F. Coffin, "Part-Through and Compact Tension Corrosion Fatigue Crack Growth Behavior of Carbon Steel in High-Temperature Water," General Electric Corporate Research and Development Report No. 81CRD159, July 1981.

19. T. A. Prater and L. F. Coffin, "Crack Growth Studies on a Carbon Steel in Oxygenated High-Pressure Water at Elevated Temperatures," General Electric Corporate Research and Development Report No. 81CRD067, April 1981.

20. W. H. Cullen, et al., "The Temperature Dependence of Fatigue Crack Growth Rates of A 351-CF8A Cast Stainless Steel in LWR Environment," USNRC Report NUREG/CR-3546, April 1984.

21. W. H. Cullen, et al., "Fatigue Crack Growth of A 508 Steel in High-Temperature, Pressurized Reactor Grade Water," USNRC Report NUREG/CR-0969, 1979.

22. Corrosion Fatigue Characterization of Reactor Pressure Vessel Steels — Progress Report October 1, 1982 to April 30, 1983," Babcock & Wilcox Research and Development Division, July 1983.

23. A. Saxena and S. J. Hudak, "Review and Extension of Compliance Information for Common Crack Growth Specimens," International J. of Fracture, Vol. 14, 1978, pp. 453-368.

24. W. H. Cullen, B. H. Menke, H. E. Watson and F. J. Loss, "A Computerized Data Acquisition System for a High-Temperature, Pressurized Water Fatigue Test Facility," Computer Automation of Materials Testing, ASTM STP 710, American Society for Testing and Materials, Philadelphia, PA, 1980, pp. 127-140.

25. "Standard Test Method for Constant-Load-Amplitude Fatigue Crack Growth Rates Above 10^{-8} m/cycle," Annual ASTM Standards, Part 10, Designation E647-78T. Issued annually.

26. M. L. Vanderglas and B. Mukherjee, "Growth of Surface Cracks in A 516 Gr. 70 Pressure Vessel Steel," Proceedings of the 6th SMIRT Conference, Paper No. L8/8, Vol. 9, Paris, 1981.

27. M.L. Vanderglas and B. Mukherjee, "Fatigue Threshold Stress Intensity and Life Estimation of ASTM A 106-B Piping Steel," ASME Paper 79-PVP-86, 1979, 11 pages.

28. F. Ellyin and H.-P. Li, "Fatigue Crack Growth in Large Specimens with Various Stress Ratios," J. Pressure Vessel Tech., Vol. 106, 1984, pp. 255-260.

29. W. H. Cullen, K. Torronen and M. Kemppainen, "Effects of Temperature on Fatigue Crack Growth of A 508-2 Steels in LWR Environment," USNRC Report NUREG/CR-3230, April 1983.

30. P. Yuzawich and C. W. Hughes, "An Improved Technique for Removal of Oxide Scale from Fractured Surfaces of Ferrous Materials," Practical Metallography, 1978, pp. 184-195.

31. L. A. James, "Fatigue Crack Propagation in Austenitic Stainless Steels," Atomic Energy Review, Vol. 14(1), 1976, pp. 37-86.

32. L. A. James, "Fatigue-Crack Propagation in a Cast Stainless Steel," Nuclear Technology, Vol. 26(1), 1975, pp. 46-53.

33. H. E. Hanninen, "Influence of Metallurgical Variables on Environment-Sensitive Cracking of Austenitic Alloys," International Metals Reviews, Vol. 24(3), 1979, pp. 85-135.

34. W. H. Cullen, H. E. Hanninen, K. Torronen and M. Kemppainen, "The Temperature Dependence and Environmental Enhancement Mechanism of Fatigue Crack Growth Rates of A 351-CF8A Cast Stainless Steel in LWR Environment," in Proceedings of an IAEA Specialists' Meeting on Corrosion and Corrosion Fatigue in Steam Generators and Pressure Boundary Components, Technical Research Centre of Finland, Espoo, 1983.

NRC FORM 335 (11-81)

U.S. NUCLEAR REGULATORY COMMISSION

BIBLIOGRAPHIC DATA SHEET

1. REPORT NUMBER (Assigned by DDC)
NUREG/CR-3945
MEA-2055

4. TITLE AND SUBTITLE (Add Volume No., if appropriate)
Fatigue Crack Growth Rates of Low- Carbon and Stainless Piping Steels in PWR Environment

2. (Leave blank)

3. RECIPIENT'S ACCESSION NO.

7. AUTHOR(S)
William H. Cullen

5. DATE REPORT COMPLETED
MONTH: November YEAR: 1984

9. PERFORMING ORGANIZATION NAME AND MAILING ADDRESS (Include Zip Code)
Materials Engineering Associates, Inc.
9700B George Palmer Highway
Lanham, MD 20706

DATE REPORT ISSUED
MONTH: February YEAR: 1985

6. (Leave blank)

8. (Leave blank)

12. SPONSORING ORGANIZATION NAME AND MAILING ADDRESS (Include Zip Code)
Division of Engineering Technology
Office of Regulatory Research
U.S. Nuclear Regulatory Commission
Washington, D.C. 20555

10. PROJECT/TASK/WORK UNIT NO.

11. FIN NO.
B8900

13. TYPE OF REPORT
Technical Report

PERIOD COVERED (Inclusive dates)

15. SUPPLEMENTARY NOTES

14. (Leave blank)

16. ABSTRACT (200 words or less)

Fatigue crack growth rates of A 106 Gr. C and A 516 Gr. 70 carbon steels, and A 351-CF8A stainless steel in PWR environments have been determined over a load ratio range (R) of 0.2 to 0.85, a temperature range of 93°C to 338°C, and a test frequency range of 17 mHz to 1 Hz using sinusoidal waveforms. In addition, growth rates have been determined for various orientations of the crack plane with respect to the product form. Crack growth rates in 288°C air environments have been measured in order to provide a reference baseline. These results define the magnitude of and major influences on the environmentally-assisted fatigue crack growth rates for these piping steels, and are supported by fractographic observations of the fatigue fracture surface.

17. KEY WORDS AND DOCUMENT ANALYSIS

17a. DESCRIPTORS

fatigue crack growth
piping steels
stainless steels
environmental effects
PWR environments
temperature effects
fractography
X-ray photoelectron spectroscopy

17b. IDENTIFIERS/OPEN-ENDED TERMS

18. AVAILABILITY STATEMENT
Unlimited

19. SECURITY CLASS (This report)
Unclassified

21. NO. OF PAGES

20. SECURITY CLASS (This page)

22. PRICE
S